The views expressed in this thesis are those of the author and do not reflect the official policy or position of the United States Air Force, Department of Defense, or the U.S. Government.

Dynamic Tuning of Structures for Aeroelastic Performance using Multiphase Material

Spencer Flint

A thesis
submitted in partial fulfillment of the
requirements for the degree of

Master of Science in Aeronautics and Astronautics

University of Washington

2023

Reading Committee:
Ed Habtour, Chair
Dario Di Maio, Chair
Jeffery Lipton

Program Authorized to Offer Degree:
William E. Boeing Department of Aeronautics and Astronautics

University of Washington

Abstract

Dynamic Tuning of Structures for Aeroelastic Performance using Multiphase Material

Spencer Flint

Co-Chairs of the Supervisory Committee:
Professor Ed Habtour
William E. Boeing Department of Aeronautics and Astronautics

Professor Dario Di Maio
Faculty of Engineering Technology, University of Twente, The Netherlands

This thesis reports the dynamic performance of aerospace structures with embedded multiphase materials with tunable stiffness and damping parameters. Aerospace structures face the harmful effects of environmental and operational damage due to (i) mechanical stresses generated by vibrations; and (ii) thermal stress buildup from aerodynamic heating. This has negative effects on performance. This study proposes a novel method for mitigating both while maintaining desirable flight characteristics at less stress-inducing conditions. The proposed process would redirect thermal energy generated from aerodynamic heating to create internal pressure by leveraging the expansion that occurs by phase change in specific materials. A proof of concept is demonstrated that the dynamics of an aerospace structure can be programmed to adapt to counter vibratory loads by manipulating the thermal pressure of the multiphase material. To this end, the multiphase material reduces the intensity of the kinetic and thermal energy simultaneously. Experimental tests are presented to characterize the multiphase materials, demonstrate stiffness and damping tuning with heat, and provide a comparison between using single-phase and two-phase materials in this concept. Thermal and modal simulations are then used to provide validation and a better understanding of why this concept works. Results show that the increase in internal thermal pressure with a change

of 30K was found to increase the damping of the structure by 50% while counteracting the natural drop in stiffness that occurs with temperature increase. This demonstrates that a viable concept has been successfully developed with the potential to pave the way for novel use of multiphase materials in aerospace structures and adaptive vibration control.

TABLE OF CONTENTS

LIST OF FIGURES

LIST OF TABLES

GLOSSARY

CTE: coefficient of thermal expansion, a material property that indicates the extent to which a material expands with heating.

EMA: experimental modal analysis, a physical method for understanding and modeling dynamic behavior.

FEM: finite element method, a numerical method of systematically solving functions.

FRF: frequency response function, the vibration response in the frequency domain. Peaks in this function correspond to resonance frequencies.

MULTIPHASE MATERIAL: a material of multiple phases such as solid, liquid, and gas within a given volume. In this thesis, the material is a homogeneous mixture of silicone and wax which undergoes a transition from solid to part solid (silicone) and part liquid (wax) with heating.

SINGLE-PHASE MATERIAL: a material of one phase within the temperature range of interest. In this thesis, the material is silicone.

ACKNOWLEDGMENTS

I would like to thank my advisor and committee Professor Ed Habtour, Professor Dario Di Maio, and Professor Jeff Lipton for their guidance and support in my efforts towards completing this thesis. Thank you all for your patience and assistance throughout the course of my research. Additionally, I owe my thanks to each and every member of the Illimited Lab who has supported me throughout my studies at the University of Washington.

Chapter 1
INTRODUCTION

It is remarkable to witness just in the past decade the advancements made in aerospace structural designs to overcome the environmental and operational dynamics that aircraft experience. In structural design, the main focus is typically on optimizing the aerodynamics and stability of the aircraft while withstanding harmful dynamics such as turbulence, flutter, limit cycle oscillation, or nonlinear modal coupling Habtour et al. (2019). These dynamics often lead to structural damaging Habtour et al. (2022), instability of the vehicle, or acoustic radiation. For example, wing flutter occurs when the vibration frequency of the aircraft reaches its resonance. Ideally, a higher level of damping can be designed into the wing to minimize this effect. This can also be achieved by designing the wing to have a higher resonance frequency, adjusting the aircraft speed, or morphing the composite structures using the heat generated from turbulence.

1.1 Motivation

Supersonic aircraft are typically optimized for cruising speeds and therefore must make compromises at slower speeds where takeoff, landing, and transition to and from cruise occur. If structures in an aircraft were able to automatically adjust for the specific supersonic or hypersonic flying regimes, controls complexity could be reduced and the aircraft would be able to perform at a higher level across multiple regimes, rather than trying to be either a jack-of-all-trades or configured only for high speed flight.

Starting with a simplified wingbox profile, Fig. 1.1, we can attempt to change the modal properties of the structure based on the environment. As heat is generated massively at high

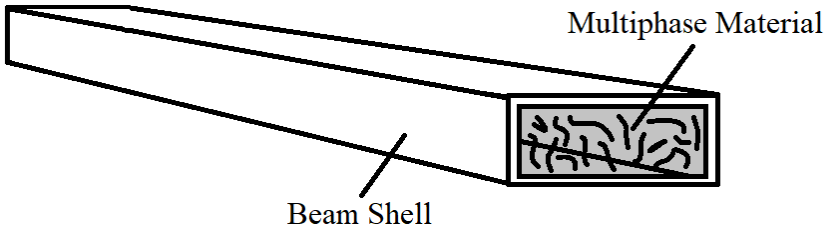

Figure 1.1: Modal testing specimen embedded with multiphase material. Simplifies the shape of a wingbox for improved test results.

supersonic speeds, this could be leveraged to create stresses in the structure that would result in changes in stiffness and damping. In order to accomplish this, a material that expands greatly upon phase change could be used to create an internal pressure and tension with this heat energy. This would make the body more rigid, similar to an inflating balloon. This was tested using a known high-expansion material of wax at lower temperatures and on a smaller scale as a proof of concept.

While this connection between material phase and dynamic phase has been explored, much less has been researched about it as a possible step forward to combating aeroelasticity challenges in hypersonic vehicles. In our study, we show that environmental thermal loads can be exploited to tune the structural stiffness and damping of a composite structure by embedding multiphase material blend of wax and silicone.

1.2 Prior Work

The field of aerospace engineering has undergone significant advances in the use of lightweight composite materials, advanced manufacturing techniques, and novel structural design in order to reduce weight and improve strength and vibration characteristics in aerospace structures. However, these technologies cannot be relied on alone in order to combat the problems discussed earlier like flutter. For example, research has been conducted to utilize control systems linked with the various control surfaces of aircraft in order to actively suppress flutter

Zhao (2009). An alternative method researched to counteract undesired vibrations was embedding shape memory material strategically within a composite wing. By applying heat to certain areas, the damping of the structure could be significantly increased with a minor decrease in stiffness Butaud et al. (2020). The shape memory approach differs from the one taken in this research effort in several ways, including our attempt to leverage thermal energy created by the environmental conditions and the use of phase change to induce pressure.

1.3 Phase Changing Materials

Past research on phase changing and multiphase materials has been conducted in the pursuit of creating powerful actuators. The potential of wax as an actuator comes from its high expansion during phase change from solid to liquid. One challenge that has been addressed in creating usable actuators is containing the wax as it becomes a liquid Mann et al. (2020). By mixing liquid wax with uncured silicone to create a single multiphase material, the mixture can be formed and even printed into shapes. After curing, these expand upon heating and return to their original form after cooling due to the elasticity of silicone Lipton et al. (2016).

For aircraft, the use of multiphase materials as a solution to vibration control will require new design decisions. There would be a trade-off between the weight increase due to additional non-structural multiphase material and the added benefits of vibration resistance and tunable aeroelasticity. This is a potential reason for there being little other research in the area. This research attempt is a proof of concept that can develop guidelines for the materials that may be later invented for aerospace. The primary focus of most research in similar areas is on alternative methods for affecting a structure's vibration characteristics. For example, a few researchers have investigated filling structures with a shear-thickening fluid like a mixture of corn starch and water to passively dampen and stiffen the structure when vibration frequencies increase but have little effect at lower frequencies Gürgen and Sofuoğlu (2019). Other research has involved polymer composites embedded in nanotubes or structural design focused on the micro-scale to create specific effects like vibration damping Agnese and Scarpa (2014); Arani et al. (2013).

1.4 Vibrations

Because this research reports on the modal characteristics of a multiphase structure, a general introduction to vibration is required. First, the vibration of cantilevered structures will be discussed. A cantilevered beam is one anchored, or fixed, at one end and free at the other. Cantilevered beams are chosen in this work for analysis because the structure of interest, an aircraft wing, is a cantilevered structure. Upon excitation, the tip of a cantilevered beam will oscillate in response. The response pattern of a beam is predictable based on material and structural design.

As for the case of flutter, when the excitation occurs at a rate similar to the natural frequency, the vibrations become increasingly large and can lead to fatigue or failure of the structure over time. Reduction of these vibrations can be achieved through forms of increasing damping or avoiding resonance by adjusting stiffness or using active control techniques as discussed earlier.

In most cases, higher temperatures lead to a decrease in vibration frequencies, primarily because of the temperature dependency of the material's Young's modulus Xia et al. (2012). This is necessary to understand because part of our research includes finding the stiffness changes of a structure with temperature.

Experimental Modal Analysis (EMA) is an instrument used for describing, understanding and modeling of the dynamic behavior of a structure. These experiments are important to determine the vibration levels and characteristics within the beam structure. The modal response in the time domain can be converted to a Frequency Response Function (FRF) that describes the dynamics of the structure tested. From the FRF, the natural frequency and damping coefficient can be retrieved. In our case, the experiments were conducted at various temperatures for comparison. Conducting modal analysis experimentally also assists in verifying the predictions made from theoretical calculations and numerical models.

1.5 Thesis Organization and Overview

The primary goal of this work is to determine the feasibility of using multiphase material to control stiffness and damping based on thermal loads. Additionally, the results presented here are meant to pave the way forward for future research. In order to reach this goal, several steps are required. As shown in the flowchart in Fig. 1.2, the tests that will directly help determine the effectiveness of changes in stiffness and damping with heat are numerical modal analysis and experimental modal analysis.

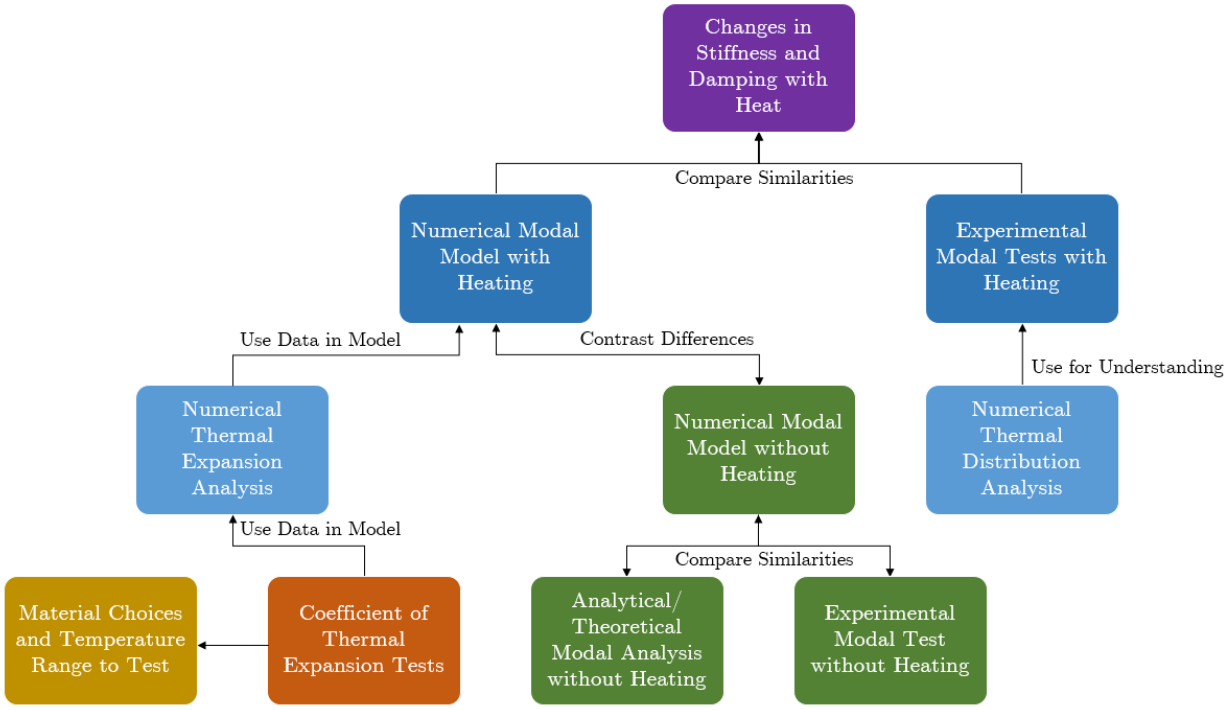

Figure 1.2: Flowchart of numerical, analytical, and experimental testing required to achieve a full understanding of the performance of this proof of concept.

Both numerical and experimental analyses were conducted on a rectangular beam structure to simulate a wingbox across several heating states in order to see how the heat affects the vibration. The structure was comprised of a hollow composite beam filled with the mul-

tiphase material in question. These tests were compared to one another in order to see how an idealized model would perform versus the concept in the physical world.

While temperatures, stresses, and strains are known throughout a numerical model, only what is measured by instrumentation is known from an experimental test. Because of the heating process used for the experiment, the distribution of temperature was not uniform throughout each specimen. In order to further understand the results of the modal experiment, a thermal model was run to simulate and predict the heating process and the thermal distribution during the experiment.

In order to find resonance frequencies with numerical modal analysis, the states of thermal stress and strain were generated by a thermal expansion model with temperature inputs. To calculate these stress and strain states, material properties such as the Young's modulus and coefficient of thermal expansion (CTE) were required. While the Young's modulus, density, and other material properties of the composite beam were known and that of the multiphase material could be found using the rule of mixtures, the CTE of the multiphase material was unknown. This is because the CTE of the multiphase material is a combination of silicone and wax, but the wax undergoes a phase change in the tested temperature range. While this is the primary desired characteristic of the multiphase material, it complicates the process because it means that the CTE had to be estimated through experimental measurements. The experimental tests that estimated the CTE of the multiphase material also showed what temperature range should be used for the modal tests, as the phase change needed to be captured. Lastly, because the CTE tests were conducted using multiple compositions of multiphase material, the weight percentage of wax and silicone used in later analyses was determined by these tests.

The remaining tests shown in Fig. 1.2, helped verify the models and experiments. Without heating, the model was able to be compared with its heated counterpart to see what differences in vibration occur from a cool to a hot state. In addition, this allowed for a direct comparison between theory, model, and experiment at a room temperature, unstressed state.

In Chapter 2, the numerical models and theoretical calculations are covered. The setup

and results are included for both the numerical thermal expansion and thermal distribution analyses because their results primarily pertain to other parts of the study. In Chapter 3, the setup and testing of experiments are specified. In Chapter 4, the remaining simulation results and the experimental results are presented, alongside a discussion of these results. Chapter 5 includes the conclusion of the study as well as a suggested path forward with future work.

Chapter 2

ANALYSIS

A key part of this research effort was to develop the required models for understanding and tuning the multiphase material properties as a function of temperature.

2.1 Structural Design

The structural design for the numerical and analytical modeling efforts was based on the specimens used in the experiments. The model was comprised of a hollow rectangular beam made from carbon fiber composite with inner dimensions 60.0 x 5.0 x 2.5cm^3 and a thickness of 1.9mm and a silicone and wax multiphase mixture inside, as shown in Figure 2.1. A small 5.0mm thick flat plate covers each open end, also modeled using carbon fiber. Inside the beam assembly was a heater 1.0cm in width that runs the full 60.0cm length.

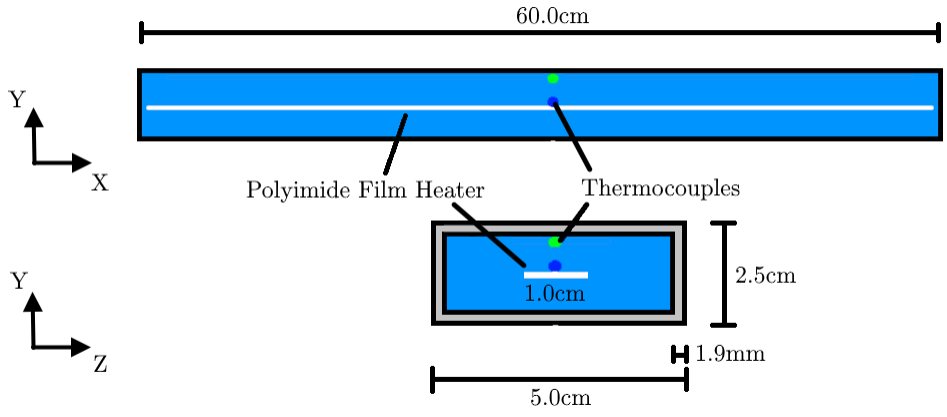

Figure 2.1: Structure dimensions and instrumentation used in models and experiments as shown from the side and from the end.

Figure 2.2: Cantilever beam in vibration.

2.2 Estimating the Modal Stiffness

To give an analytical comparison to numerical and experimental methods, the natural frequencies of the beam structure were estimated. This was achieved using cantilevered, or fixed-free, boundary conditions. One assumption made was that the wax and silicone mixture and the carbon fiber composite were both isotropic, or had a symmetric modulus of elasticity in all directions. A second assumption was that the free-end cap could be treated as a point mass. This was possible due to the cap's relatively small second moment of inertia and distance from the fixed end. It also significantly simplifies the calculation required to estimate the natural frequencies. The Young's modulus and density for the carbon fiber and multiphase material used in these calculations are found in Table 2.1.

In this analysis, any out-of-plane effects, torsion, and shear were ignored. Stretching of the beam's neutral axis is also insignificant H and Pai (2008). A cantilevered beam's natural frequencies for each n^{th} mode are expressed by:

$$\omega_n = (\beta_n L)^2 \sqrt{\frac{EI}{mL^4}} \tag{2.1}$$

where β_n is the eigenvalue for the n^{th} mode, L is the length of the beam, E is the elastic, or Young's modulus, I is the second moment of inertia, and m is the distributed mass of the beam. The first three values of βL are $\beta_1 L = 1.875$, $\beta_1 L = 4.694$, and $\beta_1 L = 7.855$ H and Pai (2008).

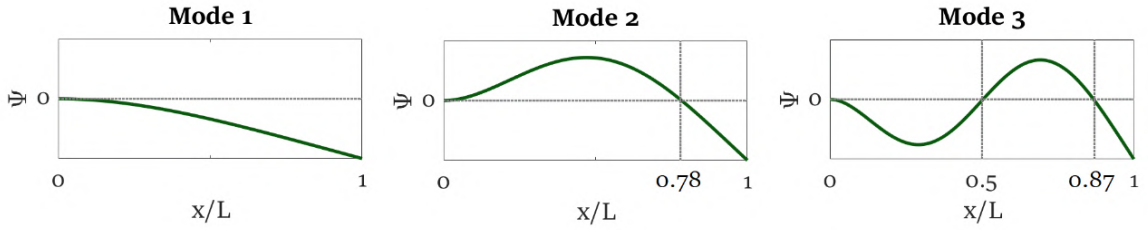

Figure 2.3: First three mode shapes for a two-dimensional cantilevered beam. The y-axis demonstrates the shape of the beam while the x-axis shows the normalized distance from the fixed end H and Pai (2008).

In order to account for the multiphase material inside of the carbon fiber beam, the values EI and m can be calculated as follows:

$$EI = E_c I_c + E_p I_p \tag{2.2}$$

$$m = \rho_c A_c + \rho_p A_p \tag{2.3}$$

where the subscript c signifies the carbon composite and p signifies the multiphase material, ρ is the density, and A is the cross sectional area Whitney (1999). The values obtained from these calculations can be found in Table 2.2 as compared with the beam model discussed later.

2.3 Modeling Overview

After the coefficients of thermal expansion were determined experimentally, the analysis phase continued with the necessary thermal and vibration models using this data. In addition, analytical calculations could be performed to compare with the numerical data. The models and tests discussed in this section are shown highlighted in Fig. 2.4.

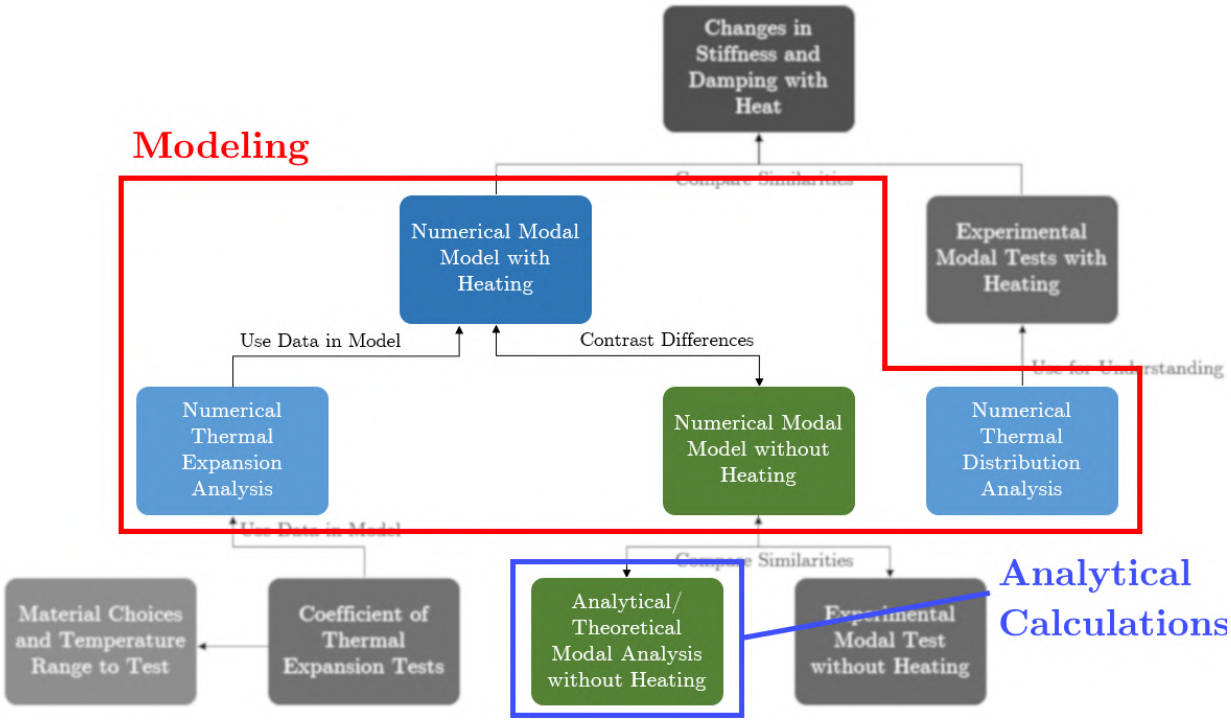

Figure 2.4: Flowchart of numerical and analytical testing and calculations focused on in this section.

2.4 Setup of Numerical Modal Model

The finite element method (FEM) was used to estimate the first two natural frequencies' mode shapes for the structure as a function of the temperature change of the internal multiphase material. The commercial software Abaqus was leveraged to perform the FEM models, which were conducted for three beam cases: beam (1) without multiphase material, (2) with silicone, and (3) with silicone and 15% wax filler. The objective was to examine the change in the internal pressure in the beams when the multiphase material was heated. This would mean that manipulating the internal temperature of the multiphase material would change the pressure and would enable the natural frequencies to be tuned. The beam dimensions were 600mm in length with a 25mm by 50mm cross-section. The beam material used was

a carbon fiber weave with a 45/45/0/45/45 layup. The beam was cantilevered, as shown in Fig. 2.5. The material properties used for this analysis are shown in Table 2.1. Only the properties necessary for the modal and thermal expansion simulations are included here, as other inputs would provide no benefit to the model. These assume that the material acts isotropically, though this was not true in reality. It was possible to use this assumption because it simplifies the analysis and was unimportant to the focus of the model: to see the changes in stiffness due to the multiphase material expansion. Using carbon fiber as the beam material was not necessary for the desired results, other than to attempt to have the model and experimental data match.

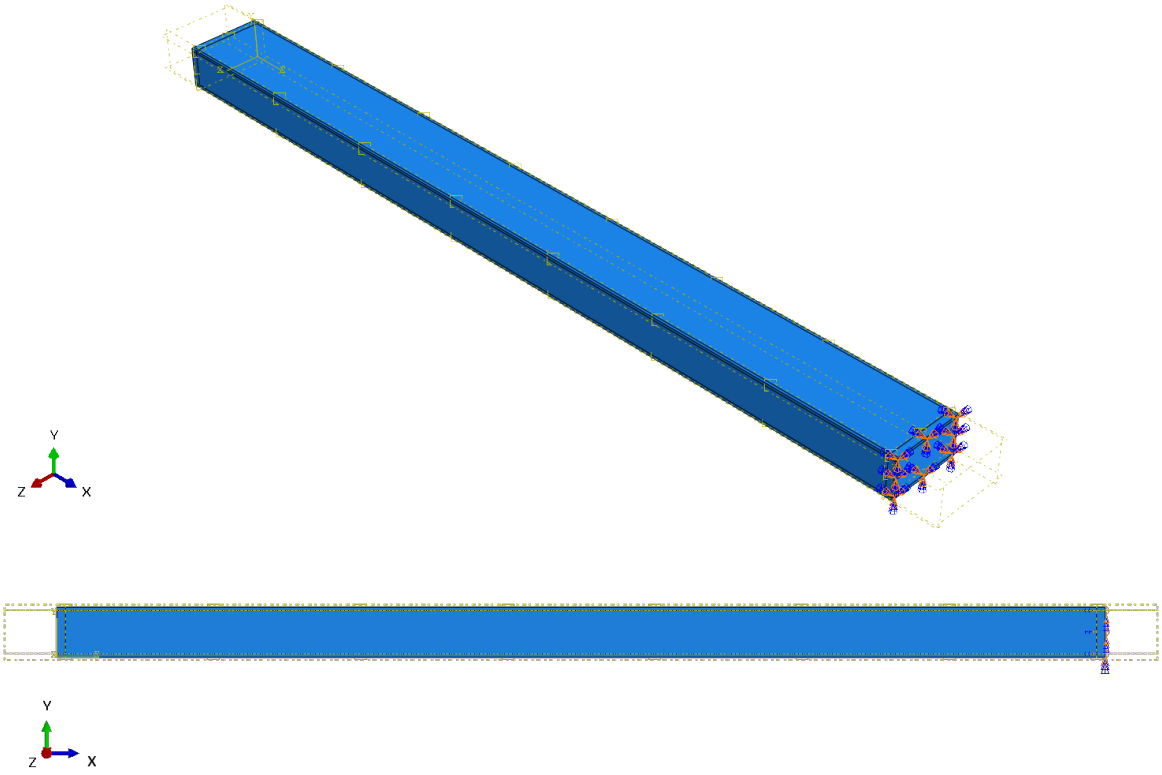

Figure 2.5: Boundary conditions for cantilevered beam in FEM software with isometric and side views.

	Carbon Fiber	Silicone, 0% Wax	Silicone, 15% Wax
Elastic Modulus (Pa)	$8.41\text{x}10^{10}$	$1.35\text{x}10^{6}$	$1.18\text{x}10^{6}$
Density (kg/m^3)	1522	1120	1099
Poisson's Ratio (J/kg-K)	0.3	0.47	0.47
Coefficient of Thermal Expansion	0	$3.79\text{x}10^{-4}$	$9.87\text{x}10^{-4}$

Table 2.1: Material properties used in modal and thermal expansion analysis. The elastic modulus and density of carbon fiber is found in car (2023a). Its Poisson's ratio is found from car (2023b), and the CTE from car (2021). The silicone elastic modulus and density are from Mol (2023). Its Poisson's ratio is from mat (2023). The wax density is from pro (2023) and the elastic modulus from par (2023). The multiphase values are found using the rule of mixtures. The CTE for silicone and the multiphase material were found experimentally.

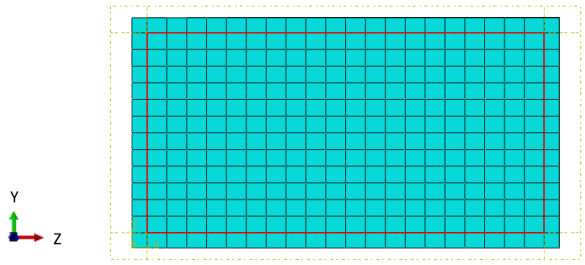

Figure 2.6: End view of mesh to show the scale of elements within FEM model. All 75152 elements are approximately 2.5x2.5x2.5mm^3, creating dimensions of 244x22x14 elements for the beam.

After creating the part and material properties in Abaqus, the beam was meshed into elements for computation. 75152 elements were used in the model of approximate size 2.5 $\times$ 2.5 $\times$ 2.5mm^3, as seen from the end in Fig. 2.6. The carbon fiber elements were general-purpose linear brick 8-node C3D8R elements. For modeling both silicone and the multiphase

material, C3D8RH hybrid elements were used due to having a Poisson's ratio near 0.5. A model using a coarse mesh with relatively few elements was created initially. The number of elements was increased in each simulation until the results converged close to the expected values, as seen in Fig. 2.8. This was a sensitivity analysis that determined the appropriate element size.

The cantilever boundary conditions were applied by fixing the nodes at one end in all translation and rotation directions. Without changing temperature and without pre-applied stresses or deflections, the resonant frequencies were found by conducting a modal analysis of the structure in Abaqus. The lowest two frequencies were reported, shown for each simulation in Table 2.2.

By not including heat in these initial models, it was possible to make a comparison to the estimated modal frequencies from analytical calculations. To help pinpoint possible errors, calculations and models were made for the carbon fiber and end caps alone, the silicone alone, and the whole assembly. In looking at the first two modes, it was found that the numerical and theoretical data lined up nicely, with a maximum percent difference of 4.5%. For the carbon fiber and end caps, the highest difference was 4.0% while for the silicone alone it was 0.51%. This demonstrates that the difference found was likely due to the end caps being approximated as point masses in the analytical calculations. Thus, the assembly and interaction between silicone and carbon fiber seemed to be working properly in the model. The first mode is in the y direction or bending towards the wider side, while the second mode is in the z direction bending towards the shorter side. These mode shapes are shown in 2.7. It is also worth noting that the addition of silicone to the carbon fiber beam drops the natural frequency by about half for both modes. This makes sense because both natural frequencies of the silicone alone were below 1Hz and essentially act as adding mass throughout the beam. These calculations were only done for silicone with no wax because the only changes that would be made in both the model and the calculations are the density and Young's modulus, thus the comparison would yield the same results as the silicone between the two.

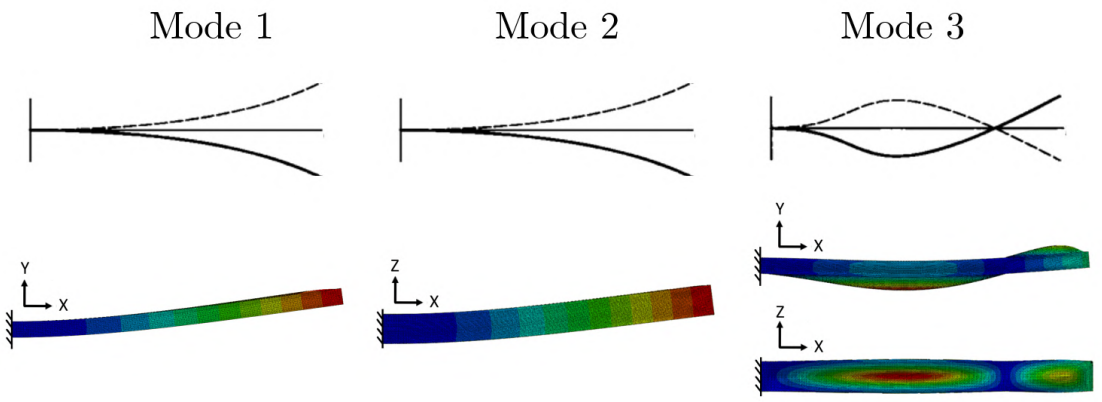

Figure 2.7: First three mode shapes of the beam sketched and as demonstrated through modeling.

	Mode	Model (Hz)	Analytical (Hz)	% Difference
Carbon Fiber	1	121.7	126.8	4.04
	2	201.4	208.3	3.33
Silicone	1	0.394	0.392	0.51
	2	0.783	0.784	0.13
Combined	1	63.7	66.7	4.50
	2	105.1	109.6	4.06

Table 2.2: Natural frequencies estimated for the empty carbon fiber beam, silicone alone, and the beam with both combined, as found through the model and analytically.

2.5 Modeling the Thermal Expansion

By calculating stresses and strains at a set temperature with a numerical model, each initial state needed for the vibration models with heat were found. This was done by taking the same structural model in Abaqus and including the CTE values in the material properties in order to be able to calculate how much each material should expand. The contact created

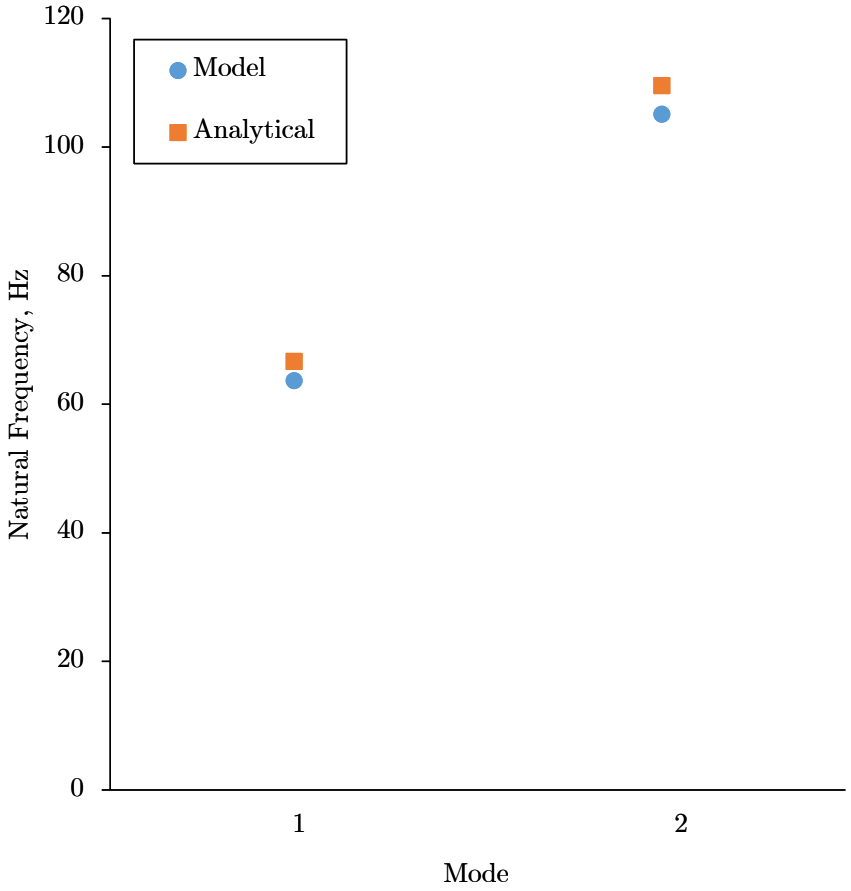

Figure 2.8: Differences in natural frequencies for the first two modes between analytical calculations and modal simulation. These values are for a room temperature of 20°C.

between the beam shell and multiphase material in the past test allowed internal pressure created from this expansion to act on the beam. From this pressure, the calculation of the stresses and the deformation were also possible.

The numerical thermal expansion simulations were the first step used in Abaqus that were then fed into the second step of modal analysis. These simulations demonstrated that for the same temperature increase, there was a greater amount of expansion in the beam for the multiphase material with wax, as seen in Fig. 2.9. This was to be expected as the

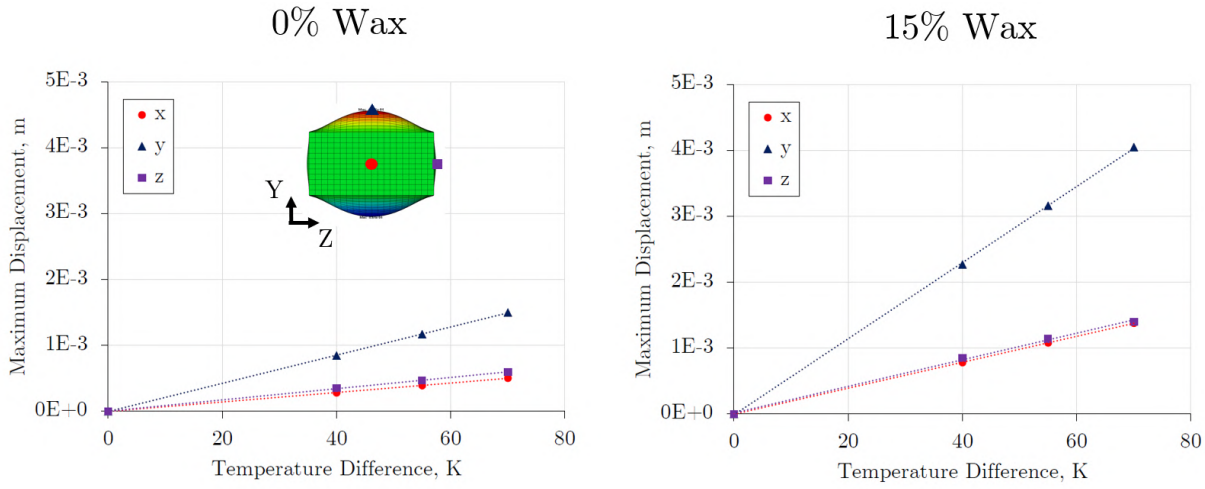

Figure 2.9: Maximum displacement in the x, y, and z directions with respective locations plotted on the deformed model. All trends were linear with respect to the temperature difference, and the wax model demonstrated a significantly higher expansion.

multiphase material has a higher CTE value.

In order to test for natural frequencies at the higher temperature deformed states created in the thermal expansion model, the same modal analysis was conducted as a second step to the expansion model. The remainder of the analysis was the same.

2.6 Modeling the Thermal Distribution

In order to estimate the distribution of temperature during the experimental tests, a model of the thermal distribution was created. The structural model for thermal distribution analysis was the same as the thermal expansion and modal models with a few key additions. Element sizes were the same, but the element type used for all elements was DC3D8, a linear 8-node heat transfer brick. Included inside the beam assembly was a heater 1cm in width that ran the full 60cm length. This was done as an alternative to setting a specific temperature for the entire internal material as in earlier models. These models were kept separate for simplicity and a clearer understanding of the results. Finally, material properties were added for heat

transfer such as thermal conductivity and specific heat capacity. These values are shown in Table 2.3.

	Carbon Fiber	Silicone, 0% Wax	Silicone, 15% Wax
Thermal Conductivity In-Plane (W/m-K)	5	0.21	0.21
Thermal Conductivity Transverse (W/m-K)	0.5	0.21	0.21
Specific Heat Capacity (J/kg-K)	1130	837.0	711.8

Table 2.3: Additional material properties added to be used in thermal distribution analysis. The thermal conductivity and specific heat of carbon fiber are found in car (2023c). The silicone thermal conductivity is from Mol (2023). The wax thermal conductivity and heat capacity are from wax (2023). The silicone heat capacity is from mat (2023). The multiphase values are found using the rule of mixtures.

In order to simulate the heating process, a heat flux matching the heater's rated power output was applied to the surface of the heater in the model. All three planes of symmetry were used in this simulation to increase the computation speed. This was possible because, in all three directions, the beam was symmetric across the mid-plane. A transient heat transfer analysis was conducted which gave the thermal distribution throughout the heating process. The final steady-state thermal distribution is shown in Fig. 2.10 and Fig. 2.11.

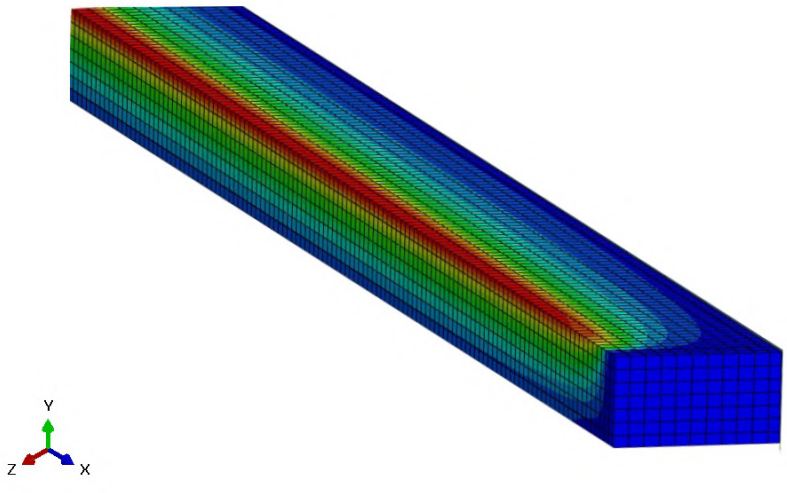

Figure 2.10: Modeled thermal distribution on a one-eighth symmetric corner of the beam. The hottest temperatures are in red and the coldest are in blue.

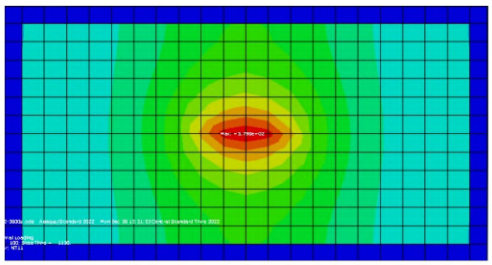

Figure 2.11: Modeled thermal distribution inside the beam at a cross-section. The hottest temperatures are in red and the coldest are in blue.

Chapter 3

EXPERIMENTAL SETUP

Altogether, the experiments conducted demonstrated the effects of temperature on stiffness and damping and the potential effectiveness of this concept in the aeronautical industry.

3.1 Estimating Coefficient of Thermal Expansion of Multiphase Materials

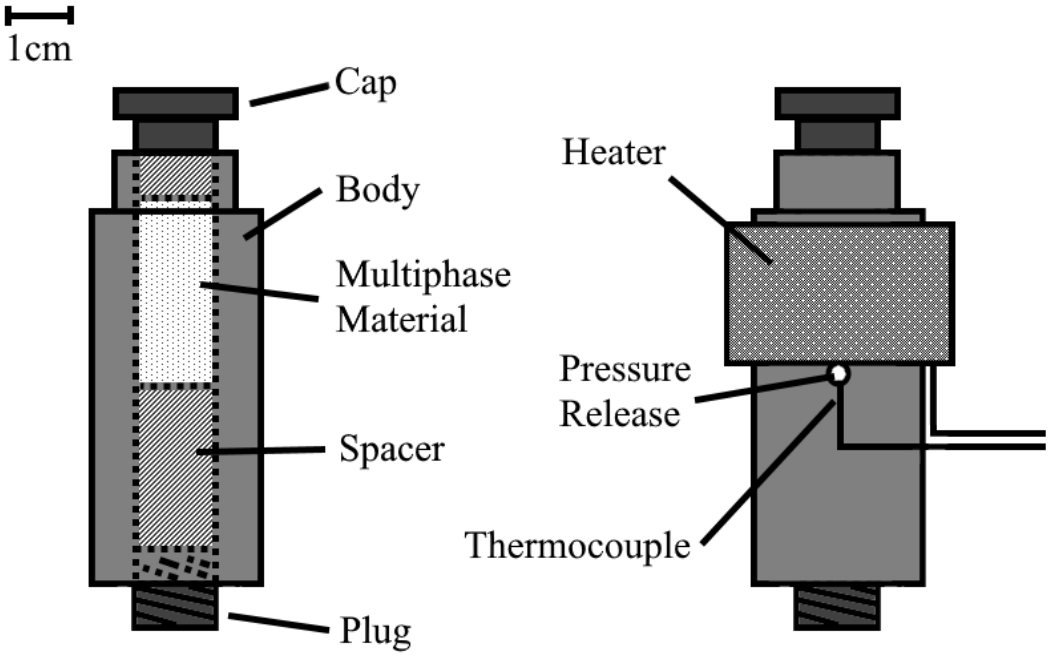

Figure 3.1: CTE testing setup comprised of a metal capsule, cap, spacer, and plug for easy access. As the multiphase material expanded, it was forced to push the loose cap on top upwards so the displacement could be measured.

In order to conduct analyses using the new multiphase materials, certain properties of these materials needed to be known. While most physical properties like the modulus of elasticity could be found easily by averaging each component's modulus using the respective percentages in the rule of mixtures, others had to be found through experimental methods. For this study, one of the most important properties of these materials was the coefficient of thermal expansion (CTE). The CTE is a measure of how much a material expands under thermal loading. Here, a high CTE was ideal in order to produce the highest possible internal pressure with heat energy. This high pressure was hypothesized to correspond to a high increase in stiffness for the overall structure. A primary goal of these tests was to determine what weight percent of wax and silicone would work best for later modal testing. This was important because the specimens needed for the modal testing required a large amount of multiphase material and only so many could be manufactured.

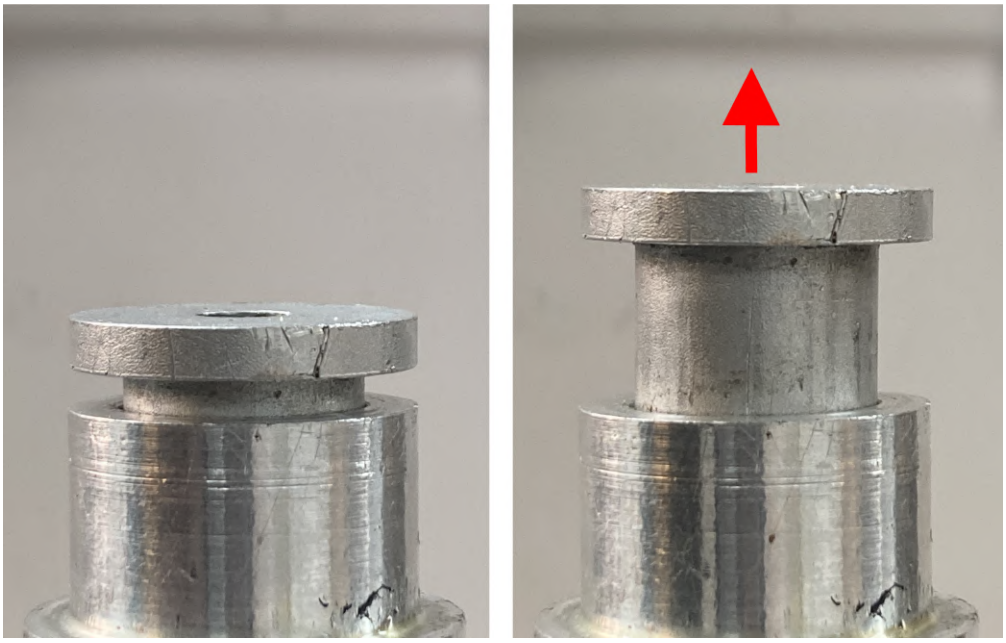

Figure 3.2: Expansion of multiphase material inside of CTE testing apparatus under thermal loading, as seen by the top piston moving upwards. This displacement was measured to assist in calculating the CTE for the material.

In order to find the CTE for each composition of multiphase material, small specimens were made to be tested for expansion in an aluminum chamber with a piston, with the expansion of this piston shown in Fig. 3.2. This configuration confined expansion to one direction allowing a more straightforward measurement of the CTE. By determining the rate of the linear thermal expansion from the cap movement, the CTE for each material at each test point was found.

$$CTE = \frac{1}{L}\frac{dL}{dT} \tag{3.1}$$

3.2 Instrumenting for the Coefficient of Thermal Expansion

The test setup used is depicted in Fig. 3.4, 3.5, and 3.3. For the test, each specimen was heated at a constant rate of 1.87°C per minute while the expansion of the piston was measured. This rate of heating was chosen to be slow enough to give each specimen time to reach a near-uniform temperature.

Figure 3.3: CTE testing chamber clamped in a vise without insulation for demonstration purposes. PID controller and thermocouple thermometer connected and shown to the side.

A heating collar wrapped around the test chamber was connected to a proportional-integral-derivative (PID) controller, shown in Fig. 3.6, that was programmed to gradually increase the temperature from 23°C to 100°C over a period of 45 minutes. This temperature range was chosen to capture well above the melting point, 54°C, of the paraffin wax used mel (2023). A thermocouple was used to measure the temperature of the multiphase material by means of a thermometer device shown in Fig. 3.7 with an accuracy of ±1.5%. In order to prevent out-gassing from affecting the results, small holes were drilled in the fixture. These were large enough to relieve this pressure but small enough to contain the material. The thermocouple was placed through one of the out-gassing holes in order to be in contact with the specimen.

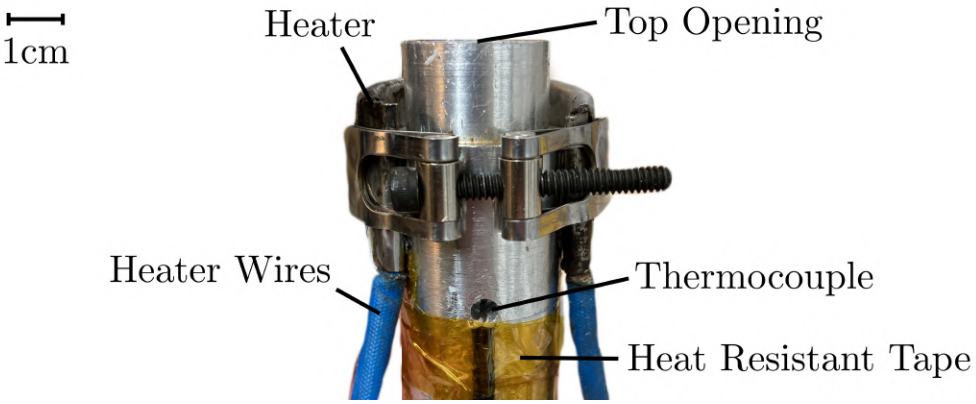

Figure 3.4: CTE testing chamber made of aluminum with heater clamped around it. The thermocouple was inserted into the side of the chamber to touch the specimen being tested. The specimen was placed inside by the opening on top, followed by the cap used to measure displacement.

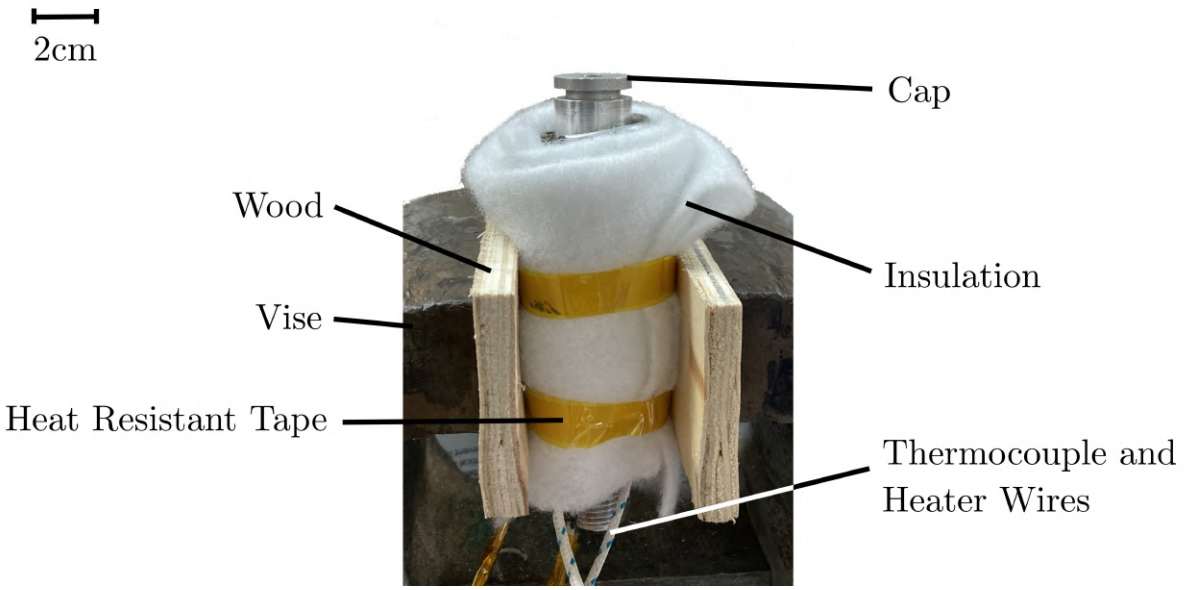

Figure 3.5: CTE testing chamber ready for testing with insulation wrapped around and clamped loosely in a vise.

Figure 3.6: Proportional–integral–derivative (PID) controller used for controlling the heater in CTE experiments. This device was set up to use thermocouple temperature readings to heat each specimen at the same linear rate.

Figure 3.7: Thermocouple thermometer used to read the temperature. Only one thermocouple was used for temperature reading in these experiments. In this case, the second is to compare with room temperature.

3.3 Making Multiphase Materials

The silicone used for these experiments was Smooth-On "Mold Max 14NV". This specific silicone was chosen due to its high-temperature rating, low viscosity, and relatively low cure time of four hours Mol (2023). The max temperature rating of 205°C means that as the material heated up, degradation of the material was insignificant to the results. In addition, the low viscosity allowed for easier pouring of the uncured silicone to create specimens. The low cure time was important in order to allow a quick turnaround from making the materials to testing. The wax used was paraffin wax which was easily obtainable, has a relatively low melting point, and has been used in previous experiments that combine silicone and wax.

In order to make the silicone, two parts (A and B) were combined by a weight ratio of 10:1 and thoroughly mixed. After mixing, the uncured liquid silicone was poured into the aluminum capsule to cure into a solid. To create the multiphase material, the wax was melted

at 150°C and added to part A of the silicone and immediately stirred until fully combined and cooled. Using a much higher temperature than the melting point was necessary because a lower one would allow the wax to solidify too quickly when poured into the part A solution. This would result in large clumps of wax in the final multiphase material making it much less accurate to assume the material was isotropic. This also would allow large amounts of wax to separate from the bulk material upon melting, rather than remaining within the matrix of silicone.

After the wax was fully mixed into part A of the silicone, part B was added and stirred in to start the curing process of the multiphase material. The mixture was grainier with a higher viscosity with the small pockets of solidified wax mixed in with the uncured silicone. Dye was mixed in to distinguish between each material composition. The mixture was then poured and left to cure. After the silicone cured, the material was removed by heating the chamber slightly to release the wax by liquidizing it. The cylinder of multiphase material was then cut down to create three separate specimens. This process was repeated for each material composition.

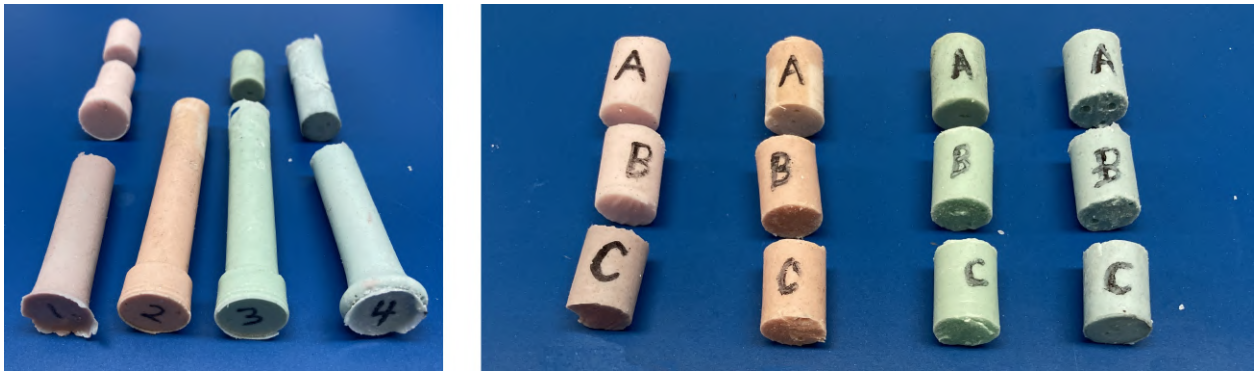

Figure 3.8: CTE specimens after curing and after being cut to size. The material compositions are ordered from least to most wax mass percent from left to right.

This test was repeated for silicone with 0%, 15%, 20%, and 25% wax by weight, with three specimens each to show consistency, shown in Fig. 3.8. These proportions of wax were

chosen for testing to maximize the material's CTE while ensuring that melted wax was kept encapsulated in the silicone Lipton et al. (2016).

3.4 Testing Process for the Coefficient of Thermal Expansion

To test the CTE of each weight percent of wax in multiphase material, each 20mm long cylindrical specimen was inserted into the aluminum chamber of the testing apparatus with the piston cap then inserted on top. The test chamber was then heated while the displacement of the cap was measured.

The PID controller ensured that each material went through the exact same heating process in testing. While the heater was running through its profile, it gathered feedback from a thermocouple to decide how much power to put to the heater and maintain its goal temperature ramp. During this process, every 2 minutes, the thermocouple temperature was recorded and the current height of the cap was recorded. This cap height was measured by using the mobile application "Skyflow" on a smartphone held fixed in a tripod which allowed photos to be taken at a fixed interval. For reference, a caliper was used to get the initial cap displacement.

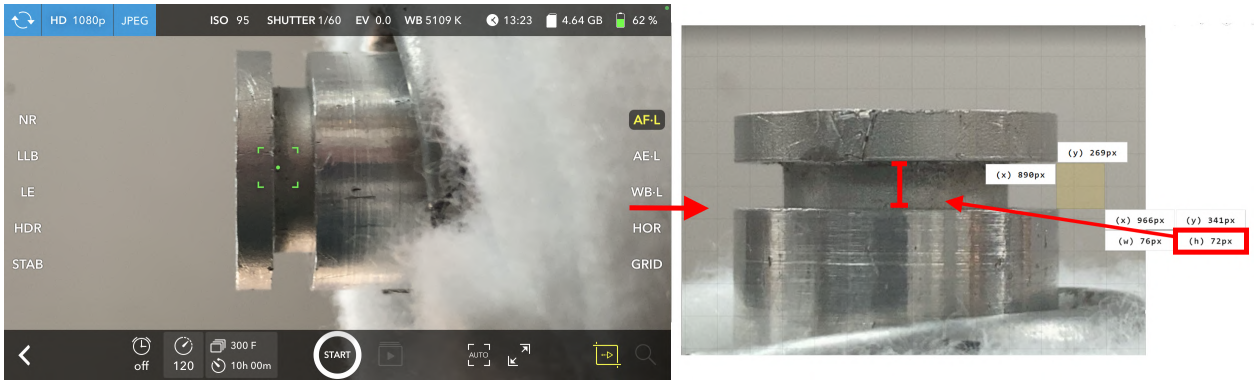

Figure 3.9: Screenshot from "Skyflow" mobile app for taking photos at a set time during CTE testing. The following screenshot is from a separate photo loaded onto a computer to be measured by pixel distance in "Page Ruler" on Google Chrome.

After the test was over, the photos were moved to a computer to find the displacement of the cap at each 2-minute interval. This was done by measuring the pixel distance between the base of the cap and the edge of the chamber in the initial photo using the Google Chrome extension "Page Ruler", as shown in Fig. 3.9. The equivalent distance of a single pixel was found by calibrating to the distance measured by a caliper. For the remaining photos, the pixel distance was converted to physical distance to find the displacement at each interval. This method was validated by measuring with a caliper after each photo was taken and comparing those measurements to the ones found from the camera. The displacement was found using a camera in order to avoid touching the cap and inadvertently moving it, producing incorrect data.

The average CTE value found for each material composition informed the material properties for the numerical models shown earlier. The CTE results also allowed a decision to be made about which composition was to be used in later testing. The composition of multiphase material with 15% wax showed the highest CTE value and therefore was used in the modal tests due to having the highest potential to produce successful tunable stiffness and damping results.

3.5 Determining Natural Frequency and Damping

In order to determine experimentally how the natural frequencies may be tuned with thermal loads, modal testing was conducted on rectangular beams filled with multiphase material, shown in Fig. 3.10. The main goals of these tests were to see what effects higher temperatures have on vibration for the multiphase material versus a comparable single-phase material. Free vibration testing was conducted on each specimen by using a modal hammer to excite the resonant frequencies, as seen in Fig. 3.11.

Rectangular beams were chosen for these experiments to emulate a wingbox from an aircraft. The beams with the narrowest cross-section available were chosen in order to keep the natural frequencies lower and more easily measurable. Carbon fiber was chosen in order to minimize weight and to avoid the heating of the multiphase material significantly softening

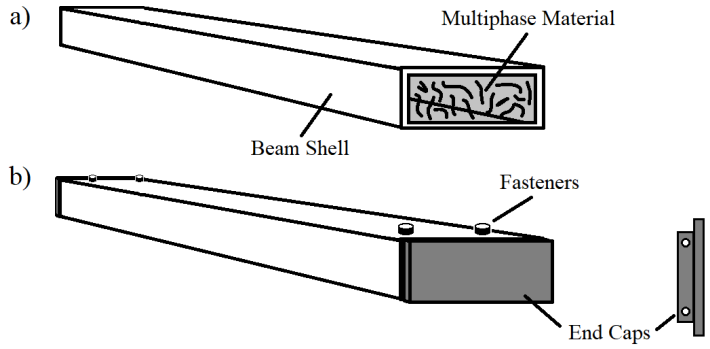

Figure 3.10: a) Diagram of beam specimen embedded with multiphase material. b) Beam specimen shown with end caps attached to demonstrate how the material was kept inside under expansion.

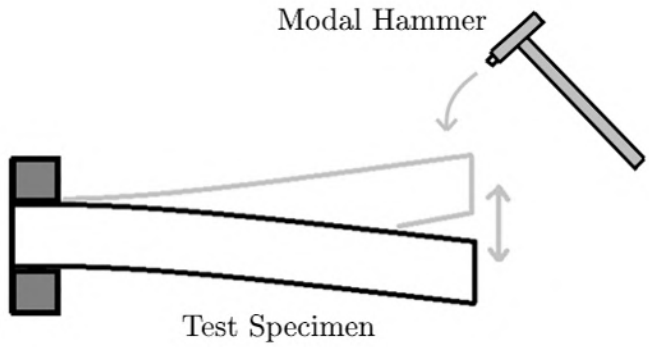

Figure 3.11: Sketch to show the motion of the first mode of vibration in beams with cantilever boundary conditions. A modal hammer is depicted in the structure excitation process.

the beam and affecting the results. A composite beam also keeps with the theme of modern supersonic aircraft design.

A design decision was made to heat the beams internally for a few separate reasons. While external heating would better simulate heat from air friction on an aircraft wing or control surface, internal heating was chosen in order to avoid unnecessary stiffness changes of

the carbon fiber beam and focus on the effects of the multiphase material heating. This was also done to maintain a higher level of consistency as less heat energy would be lost to the atmosphere. A separate but similar concept that these internal heaters simulate is heating the structure from the inside with coolant. This would allow heat generated by air friction to be strategically redirected to multiphase material in the aircraft structure. This method could also be applied to subsonic aircraft by using engine heat and would also allow the vibration properties to be actively controlled through a thermostat rather than just relying directly on the external flight regime conditions.

3.6 Instrumenting for Modal Tests

The location of thermocouples and heater included inside the beam is shown in the diagram Fig. 3.12. In Fig. 3.13 the same instrumentation is shown outside of the specimen before construction. The modal hammer used was a PCB 086C03 with 2.25mV/N of sensitivity or ±15%. The accelerometer attached to the specimen was a Dytran 3133A3 with a range of 1000g and a sensitivity of 5mV/g. To measure the modal hammer and accelerometer outputs, they were routed through a data acquisition module to a computer. The data acquisition module used was a four-channel NI 9234 with a voltage range of ±5V. The DC power supply used for the heaters was a Wanptek WPS305H with up to 30V and 5A of output. The full experimental setup is shown in Fig. 3.14. The thermal imaging camera shown was used qualitatively to ensure that heating was occurring as expected.

3.7 Constructing Modal Specimens

Three separate specimens were made and tested with cantilever (fixed-free) boundary conditions. The first specimen was filled with silicone alone, thus being comprised of 0% wax for a baseline to compare against the specimen with wax. The second specimen was filled with 15% wax and 85% silicone as the multiphase composition with the highest predicted expansion from CTE testing. This gave the best chances of inducing successful tuning of the natural frequency. The third specimen was left empty for characterization. The first two

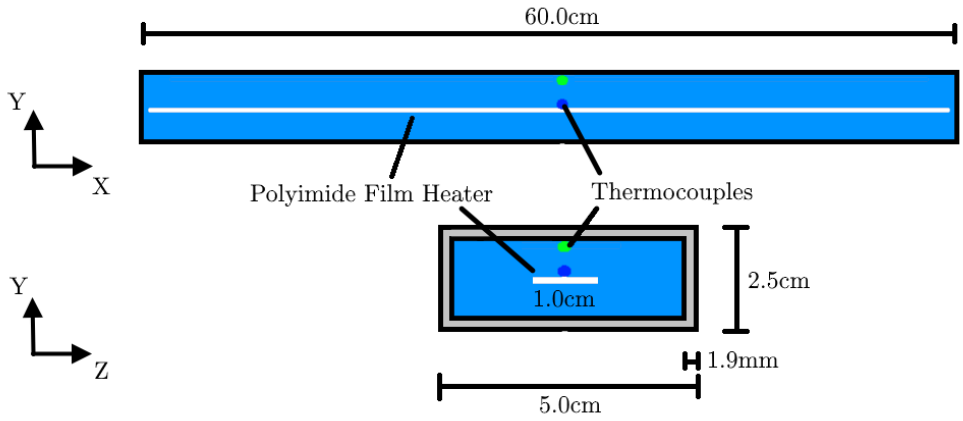

Figure 3.12: Side and end views of beam instrumentation and dimensions.

Figure 3.13: A specimen before assembly with heater wires in red and thermocouple wires in white.

specimens were equipped with heaters running down the center as well as two thermocouples in strategic locations near the center. Paired with the thermal distribution model, these two thermocouples were able to give an estimate of the distribution of temperature within the beam during testing. At either end of the specimen, a solid plastic end cap was used to keep the multiphase material in place.

In order to make each specimen, a few main parts were required: the carbon fiber beam, the silicone and wax, the end caps, the heaters, and the thermocouples. First, the carbon

Figure 3.14: Experimental modal test setup with instrumentation in cantilever boundary conditions. The accelerometer can be seen attached at the tip of the beam. Shown to the side are the DC power supply, DAQ, thermal imaging camera, thermocouple thermometer, modal hammer, and computer.

fiber beam was cut to size at 60cm in length. Next, the caps were milled out of PVC to slot 1cm into either end and keep the internal material inside. Holes were drilled in one cap for the thermocouples and heaters. These caps are shown in Fig. 3.15.

Each end cap was kept in place by two vertical bolts running through the carbon fiber beam. For these experiments, the heater was comprised of 6 individual flexible kapton heaters due to part availability constraints. Each of the 6 heaters was 10cm by 1cm and was wired to the others in parallel to mitigate the risk of a full failure. Parallel was also chosen because each heater had a maximum input of 12V and 1A, which would require 70V for a series wiring to get the same output as 12V and 6A for parallel, which was far higher than the DC power

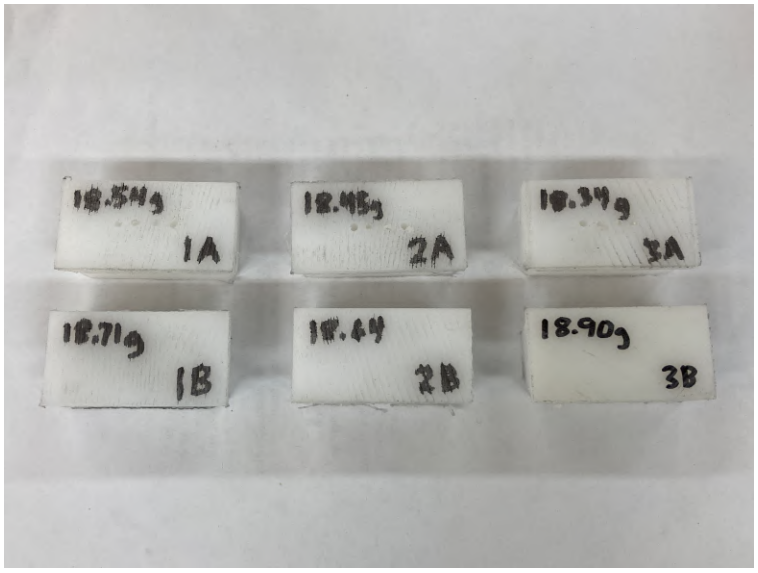

Figure 3.15: All 6 end caps used for specimens 1 through 3. Each cap was labeled with its mass in grams. Cap A was for the end of the specimen that wires come out of and had four holes drilled through the middle, while cap B was for the other end of the specimen.

supply available could handle. Two thermocouples were attached at the 30cm midpoint of the heater using kapton heat resistant tape, one flush with the heater and the other bent outwards so that it would touch the wall of the beam. The heater and thermocouple wires were then inserted into the end cap with holes and installed into the carbon fiber beam. The heater inside the unfilled beam is shown in Fig. 3.16.

Using hot glue, a seal was created to prevent uncured silicone and wax from leaking out at the cap. The final step to create the specimen was to mix and add the multiphase material. For the beam with just silicone, parts A and B were mixed by weight ratio like in creating the CTE specimens and carefully poured into the beam. The amount of silicone needed was determined by an approximate volume calculation. To prepare for the silicone pouring process, the hollow beam was held vertically in a vice lined with wood to avoid damaging the carbon fiber as shown in Fig. 3.17.

While pouring, the heater was held from either end: from the wires protruding from the

Figure 3.16: View of the heater strand inside the specimen before being filled with multiphase material. It can be seen here that the heater strand was centered well in the specimen but due to its flexibility was not kept perfectly oriented.

bottom cap and directly from the open top end. This process was made easier by holding the end with a binder clip to keep it taught and centered during the pouring process. The beam was filled enough so that when the remaining cap was installed there would be no air gap left. Excess material pushed out by the cap was left to dry to be easily pulled off after curing. The specimen with silicone and wax was produced the same with the additional step of adding wax at 150°C before part B of the silicone mixture just like for the CTE specimen creation. Each of the three specimens was labeled one, two, and three respectively to distinguish between them, as shown in Fig. 3.18.

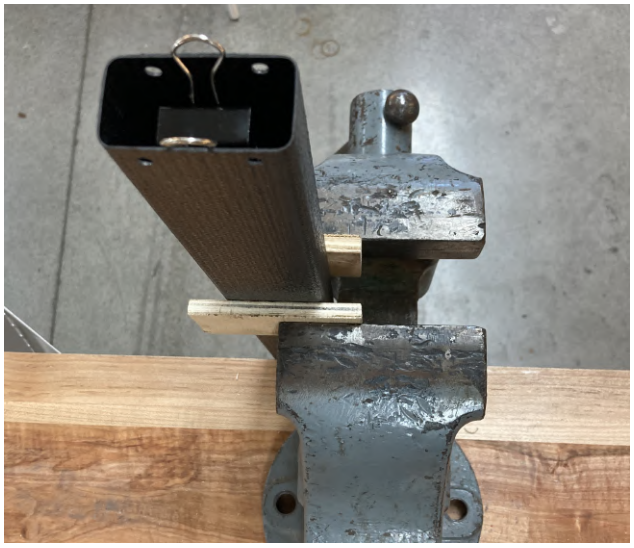

Figure 3.17: Vice holding the prepared carbon fiber specimen set up to have the uncured silicone poured in the top opening. A binder clip is shown holding the end of the heater strand in order to make sure the heater was centered properly in the beam as the mixture was poured.

3.8 Testing Process for Natural Frequency and Damping

The modal tests were conducted in a fixture that holds the specimen at the end for a cantilever boundary condition, shown in Fig. 3.19.

Free vibration modal hammer tests were conducted at various heating states by powering the heater and conducting tests every five minutes as the temperature increased. Each test involved striking the specimen with an accelerometer-measured hammer and recording the vibration response of the specimen with an accelerometer attached to it. After data was collected from both the hammer impulse and beam response, the time-based data from the accelerometers was converted to a frequency response in order to find the resonance frequencies that stood out as peaks in the data. No filtering was used in the data collection in order to avoid losing any unexpected characteristics by cutting out data.

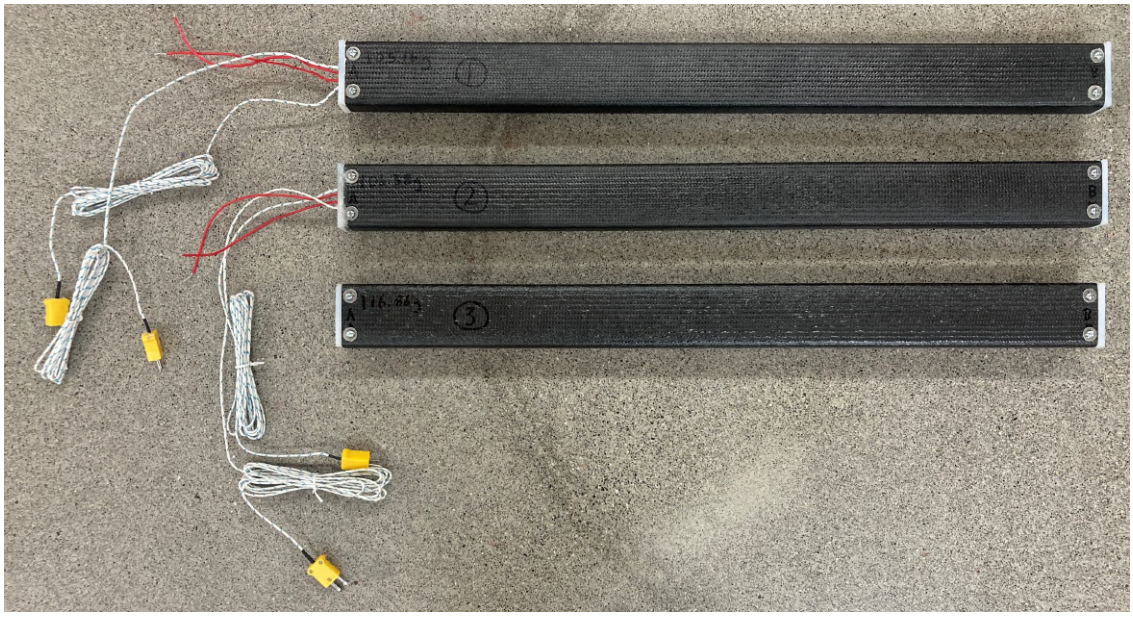

Figure 3.18: The completed modal testing specimens. The first specimen contained silicone without wax, the second had the multiphase material, a combination of silicone and wax, and the third was left hollow.

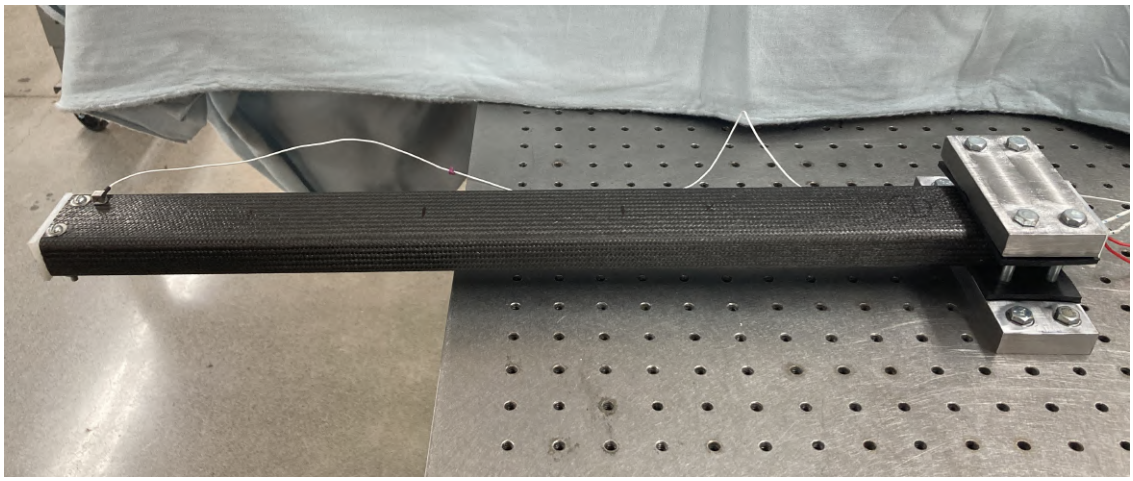

Figure 3.19: Experimental modal test setup for cantilever boundary conditions.

The thermal distribution model was used to estimate the average temperature of the specimen at each interval tested. Consistency among tests was important in order to minimize any errors that may have come about from having similar estimated average temperatures but different distributions. Ideally, a steady state would be reached for each data point, but this proved difficult and time-consuming, so a ramping of temperature was used by adding constant power throughout the duration of the test in order to test several different heating states in one heating process. The same heating process was repeated for each specimen for consistency and ease of modeling.

The results of these experiments helped determine the relationship between natural frequency versus temperature and damping versus temperature. These values showed how this adaptive multiphase structure may best be viable.

Chapter 4

RESULTS AND DISCUSSION

While the results of this study were unexpected, they demonstrated that multiphase material has strong capabilities in tuning modal properties. All tests were successful in determining the goal values.

4.1 Multiphase Coefficient of Thermal Expansion

The coefficients of thermal expansion determined by the tests conducted on each material composition show that the presence of wax within the multiphase material significantly increases its ability to expand under thermal loading. It was found that between the percentages 0% and 25% wax by mass, 15% has the highest CTE. With that said, the results from the two higher percentages show only slightly lower CTE values with standard deviations that overlap. This can be seen clearly in Fig. 4.1 which shows the averaged results from all tests conducted. These results are for the temperature range 60°C to 95°C.

As discussed in Chapter 3, the measurements for the CTE experiments were found by determining the linear displacement of the constrained silicone or silicone and wax mixture. This was done by measuring how much the cap had moved from its initial position. To find the CTE at each point, the displacement was divided by the initial length of the multiphase specimen, which was then divided by the change in temperature of the specimen, or $\frac{1}{L_0}\frac{dL}{dT}$. This value tells proportionally how much the length changes for each unit of temperature, hence why it is the linear coefficient of thermal expansion.

While it was hypothesized that the highest percentage of wax would show the highest CTE, the lowest non-zero percentage tested ended up demonstrating the highest CTE. It is possible that the true trend is a positive slope throughout, as seen in Fig. 4.1 that this is

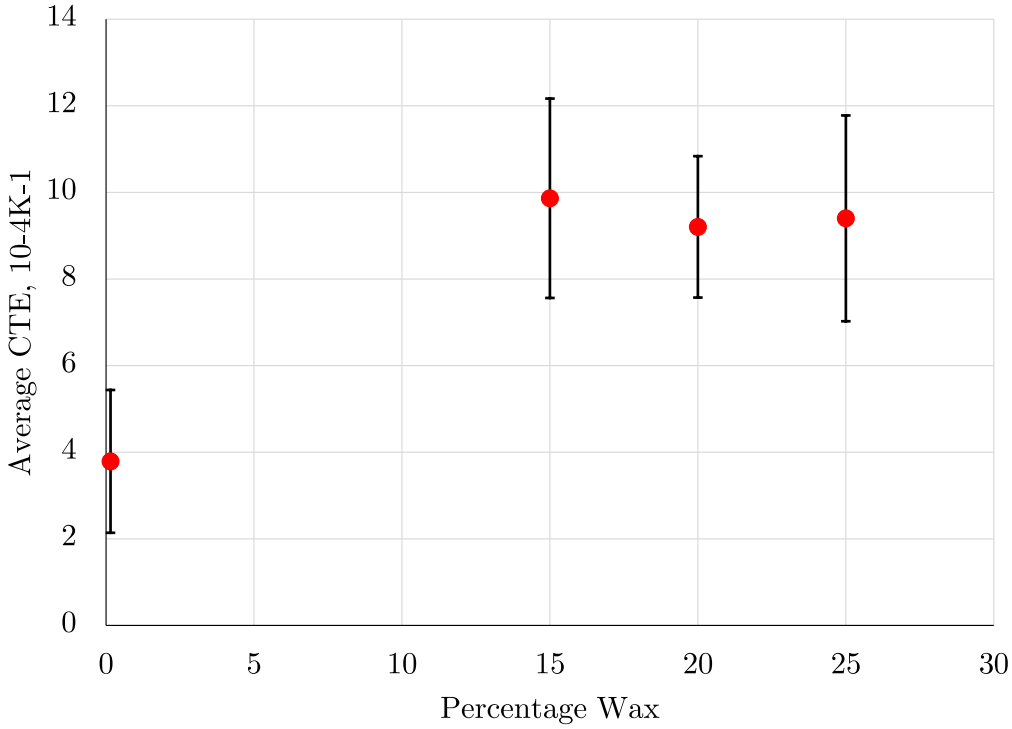

Figure 4.1: Average material coefficient of thermal expansion compared with wax percentage by mass. Bars indicate the standard deviation for each data point.

well within the standard deviation. Further testing in the range of 5% to 15% and above 30% wax would be ideal to see the trend more clearly. Either way, the wax clearly has a significant contribution by over doubling the thermal expansion while comprising less than one-fifth of the material composition.

The average CTE of each specimen tested rose slightly over the temperature gradient, but each specimen individually seemed to behave differently, as seen in the top left of 4.2. One specimen had a decrease in CTE with temperature while the other two increased at different rates. Compared to the specimens with wax; however, the CTE of the 0% wax material was relatively constant. For each of the multiphase tests aside from one of the 25% specimens, the CTE rose in a similar fashion up to a change in temperature of 40K before then increasing at a slower rate. This demonstrates that the phase change of the wax created

a strong influence on the CTE, rather than the presence of the wax material itself.

The temperature range used for this study was from room temperature at approximately 23°C up to 100°C. This gives the change in temperature values seen in Fig. 4.2 from 0K to 80K. Also shown here, the temperature change range chosen of 40K to 75K for further study is highlighted by boxes. This range was demonstrated clearly in all tests, though it can also be seen that some ranges were larger. These ranges were selected because constant CTE parameter inputs were needed for the numerical models to limit complexity and reduce additional sources of error. In these ranges, the data shows that the CTE value was the steadiest. The information in 4.1 was calculated by averaging the data in these regions and finding the standard deviation.

The CTE for the specimens containing wax, with one exception, trended upwards until approximately 40K temperature difference, seen in Fig. 4.2. At this point, all tests leveled out relative to their initial response. This may be for a few different reasons, but it was hypothesized that the starting CTE was without any wax melted, hence why it was similar to the pure silicone tests. After this point, because the temperature distribution within the specimen was non-uniform, the wax at the hottest point began to melt and expand, driving up the CTE. By about a 40K temperature difference, or 60°C, just above the wax melting point of 54°C, the amount of wax hot enough to melt was much higher and the expansion rate hit its peak. By the end of the test at about 75K temperature difference, wax may still have been melting in some cooler areas, hence why the CTE had not dropped again.

There was a larger amount of deviation than expected between individual tests, even after taking time to refine the process and remove noticeable problems. One error that may not have been accounted for was the slight changes in diameter and non-uniformity between specimens. While each was created in the same mold, not every single one had exactly the same dimensions. This is inherent to the silicone-making process. Smooth-On, the company that makes this silicone, also reports that it is possible for residual moisture and alcohol to be trapped as a by-product of the curing process.

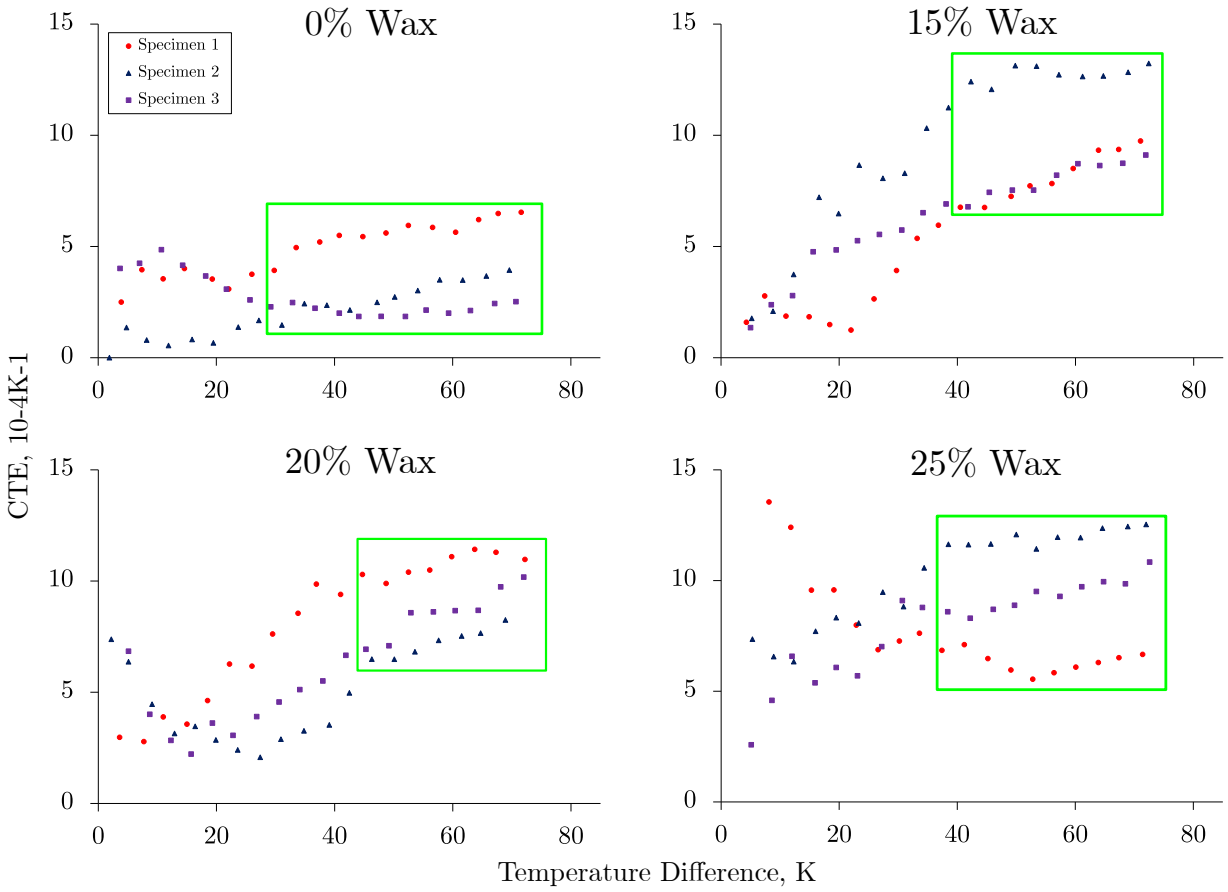

Figure 4.2: Coefficient of thermal expansion data for each percentage of wax by mass tested. Each box shows the areas where the CTE is relatively consistent across a temperature range. This data set shows a total of 12 specimens tested; they are labeled 1, 2, and 3 for each weight percent of wax.

4.2 Numerical Modal Analysis

By testing multiple temperatures in the numerical model, it was possible to see changes in the structure's stiffness. With data carried over directly from the thermal expansion model, new natural frequencies were found at each stress state. The natural frequencies with respect to their change in temperature are shown in 4.4. In all cases, the natural frequencies changed

significantly less than expected. It was hypothesized that this was because some key elements of the stiffening process may have been missed in the model. In some cases, the natural frequency decreased rather than increased. This would be expected with the softening of the carbon fiber as well as the silicone, but the Young's modulus for all materials was assumed constant to isolate the effect of the expansion on the natural frequency.

It was found that in the beam with 0% wax, the stiffness in the first mode of vibration decreased by less than 0.3% over a 75K temperature increase. In comparison, the beam with 15% wax stiffness for the first mode increased by 0.6% over the same 75K increase. This helps to demonstrate that for 0% wax composition in the beam, the stiffness changed little with temperature. While there was an increase in stiffness in the multiphase beam, it was also a relatively small change. These results show that the expansion of the multiphase material under heating has the power to change the stiffness in a more significant way than a single-phase material. This stiffness increase was expected, as the goal was to use the expansion of wax to create pressure and stress that tightens the overall structure in a way that increases stiffness. This may be caused in part because of an increase in the second moment of inertia in the y directions with temperature due to the expansion. This directly affects the stiffness as seen in the theoretical calculations discussed in Chapter 2.

4.3 Experimental Modal Tests Overview

The modal vibration experiments showed primarily that the multiphase material increases damping by 50% while retaining most of the stiffness over an average temperature increase of 30K. This was contrary to the expected outcome where stiffness would increase and the damping would remain the same. As shown in Fig. 4.5, the stiffness for the single-phase specimen without wax had a 10% drop while the multiphase specimen stiffness stayed about the same. These results show that in comparison to the single-phase specimen, the multiphase specimen was able to counteract the natural stiffness decrease with heat.

4.4 Experimental Temperature Data and Correlation with Model

Recording thermal data with the thermocouples worked as expected. The setup of having one thermocouple near the heaters and one bent so that it would touch the carbon fiber - furthest from the heaters - seemed to emulate the model well. As predicted, the thermocouple close to the heaters was always much hotter than that near the side of the beam. While the temperature values were off significantly, the proportions were as predicted thus allowing a confident estimation of average material temperature.

The data from the internal thermocouples showed primarily that the model significantly overestimated the temperatures that the specimens would reach. Because of this, the desired testing temperatures to match the numerical vibration models were not achieved, but enough change was created to at least partially melt the wax in the multiphase material and see a sizeable difference in damping. The thermocouple locations with colors matched to the temperature data are shown in Fig. 4.3. While the temperature values experimentally did not match that of the model, the general heating curve shape and the ratio between thermocouples matched well. Because of this, it was possible to use the model to estimate the average temperature of the body of silicone and wax. A ratio that takes into account the model's temperature differences between the thermocouples and the body average was determined and then applied to the experimental data. This gives a single estimated body average temperature at each point to use in order to better compare the vibration parameters with the temperature as they change.

Interestingly, while the model showed that the specimen with wax should heat up slightly faster, in the experiment the wax one heated up significantly faster, reaching a much higher maximum temperature by the end of the test, as seen in Fig. 4.3.

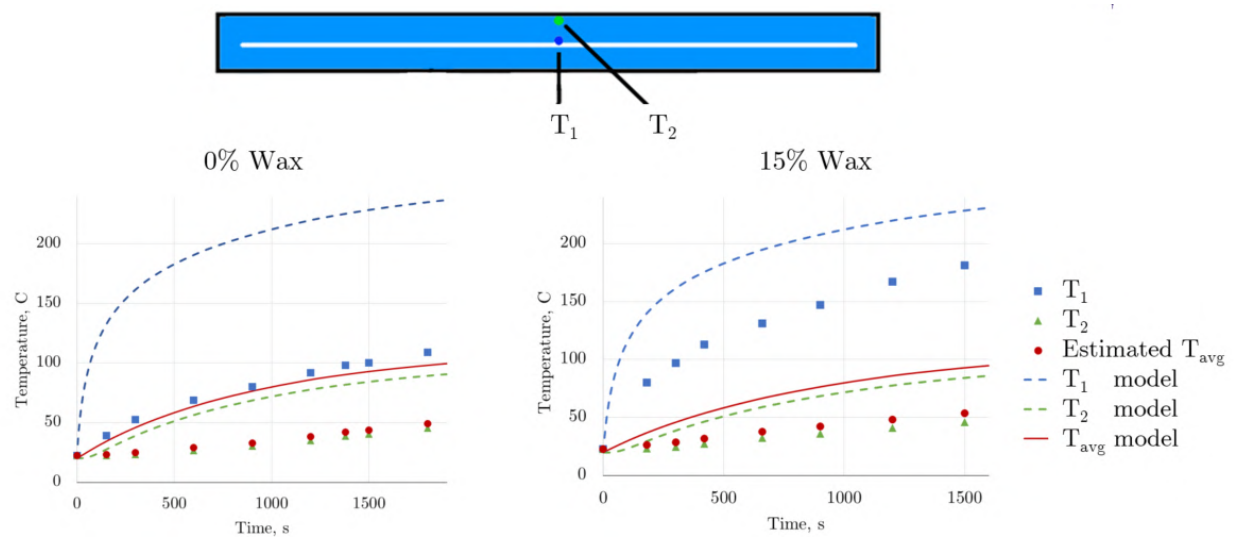

Figure 4.3: Modeled temperatures during the heating process compared to the experimental temperatures. The thermocouple locations and heater are shown in the side view above.

4.5 Experimental Modal Frequency Results

The modal experiments demonstrated the resonant frequencies only in the y direction due to the way that the modal hammer excites the specimen. With the understanding that there are mode shapes that were not tested in the z direction, for the remainder of this study, the modes discussed are 1 and 3 which are excited in the y direction.

Fig. 4.5 shows the changes in stiffness for single-phase and multiphase specimens. It can be seen that the specimen without wax had a 10% drop in stiffness in both modes tested while the specimen with wax had only a 2% drop in the first mode and a 5% increase in the third. Like the model, the relationship between natural frequency and temperature was not linear, but most tests demonstrated a trend of decreasing stiffness with increasing temperature. The fluctuation seen within each test may be in part due to the competing stiffness changes from softening of the individual materials and structural stiffening from the pressure. The main takeaway of these results is that the stiffness was maintained significantly better in the specimens with multiphase material.

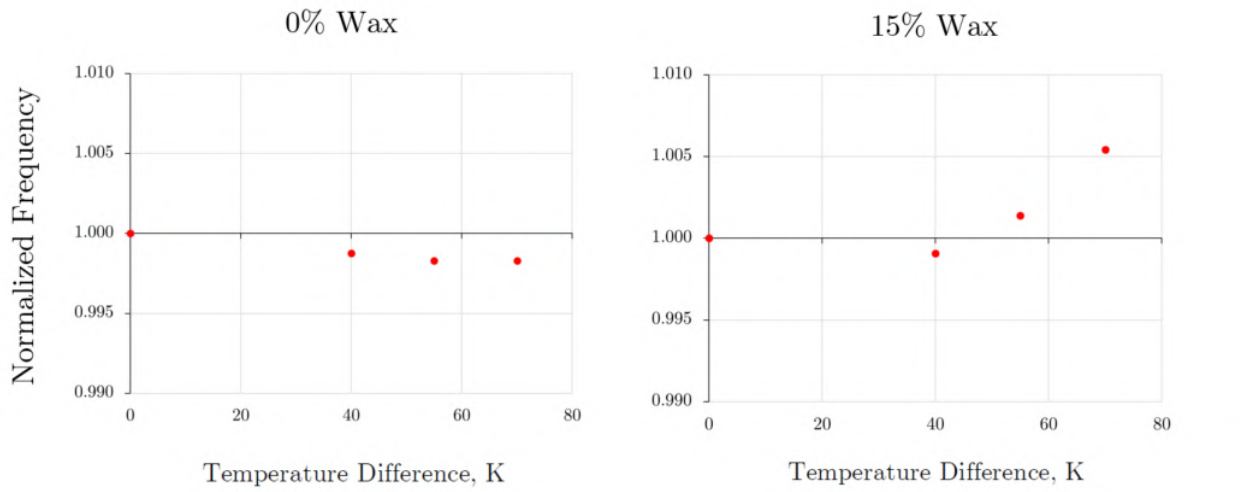

Figure 4.4: Changes in resonance frequency of the first mode in the cantilevered numerical model for 0% wax and 15% wax.

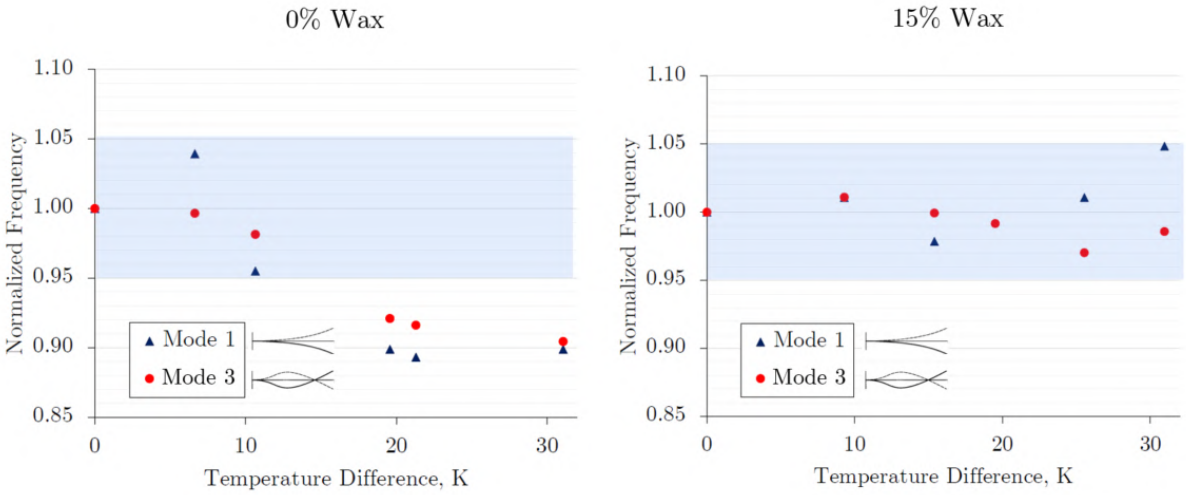

Figure 4.5: Changes in resonance frequency of the first and third modes from cantilevered experiments for 0% wax and 15% wax.

In order to find the stiffness of each specimen, the modal hammer and accelerometer data were used to gather raw data in the time history domain. No filtering was used. The time domain data was then converted to a frequency response function (FRF) by Fourier transform where each peak in the plot corresponds to a natural frequency excited in the specimen. An example of the time history data next to the FRF is shown for the multiphase beam at room temperature in 4.6.

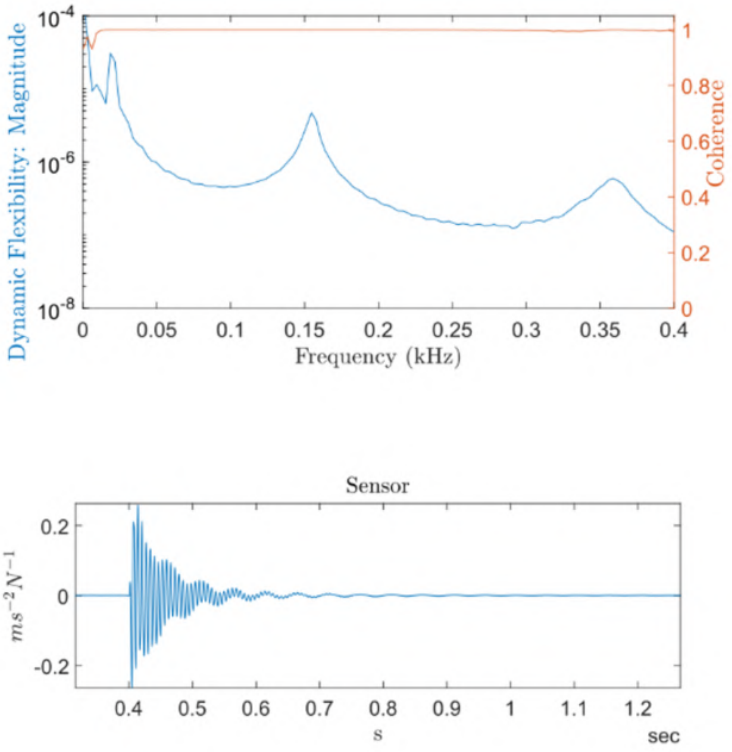

Figure 4.6: Modal frequency response function for cantilevered beam up to 400Hz showing modes 1, 3, and 5 at each peak. The respective time history domain data is shown below. This test was conducted at room temperature of 23°C on the 15% wax specimen.

4.6 Experimental Damping Results

The time history data was used to estimate each system's damping ratio. The method used was logarithmic decrement, which takes the peak in amplitude at each oscillation and calculates a decrement between it and the next one, $d = \log A_n/A_{n+1}$. The log decrements for the entire modal response are averaged to find the mean decrement, μ_d, which can be used to calculate the damping ratio:

$$\zeta = 1/\sqrt{1 + (2\pi/\mu_d)^2} \tag{4.1}$$

This damping ratio can be used to find the damping coefficient, c.

$$c = 2\zeta m\omega_d \tag{4.2}$$

In both cases, it was found that the damping coefficient of the specimens increased significantly with temperature, shown in Fig. 4.7. While the damping coefficient found for the beam without wax increased 45% in both modes, the multiphase beam showed a slightly higher increase of 50% in the damping coefficient of the third mode with just a 32K temperature increase. The first mode increased by 42%. This is surprising as even for the originally planned 75K increase in temperature, the damping was expected to stay the same or potentially decrease with the increase in stiffness in both cases.

4.7 Comparison between Model and Experimental Natural Frequencies

The difference in the first modal frequency at room temperature between the single-phase specimen and the multiphase specimen was 4.5% for cantilevered boundary conditions, with the multiphase specimen having the higher natural frequency. In comparison, the numerically calculated frequencies were very close at 0.6% difference between 0% and 15% wax. This shows that there were likely some key material property errors in the model or some wax adhesion effect that was not accounted for.

The trends observed in the model natural frequencies versus the experiments were clearly

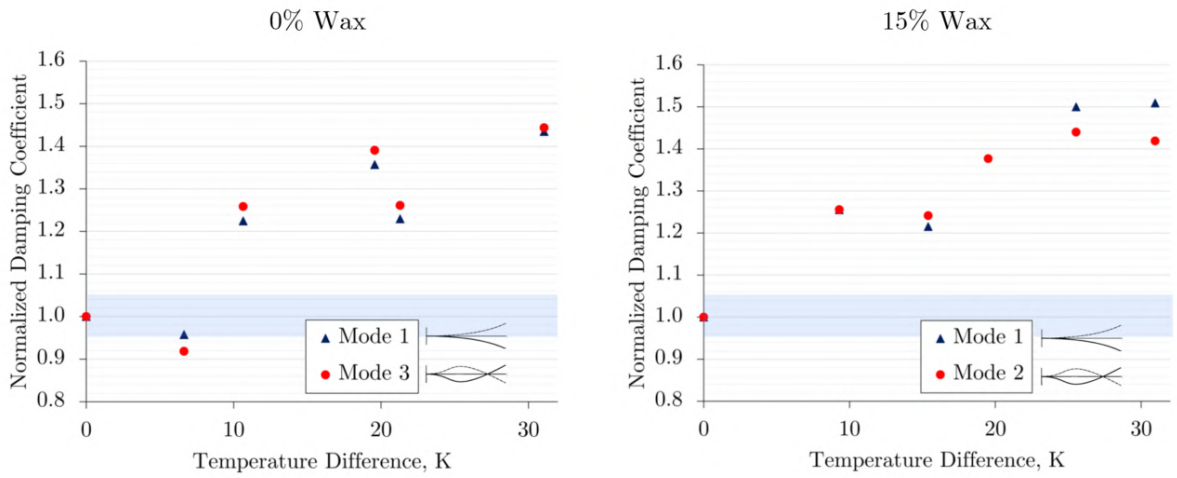

Figure 4.7: Changes in the damping coefficient of the first and third modes from cantilevered experiments for 0% wax and 15% wax.

different, but one similarity was that the multiphase material caused the frequency to increase more with temperature relative to the beam with single-phase material.

With an ability to maintain stiffness while noticeably increasing damping under reasonable heating loads, it appears that the multiphase material has demonstrated an ability to tune vibration characteristics in one respect or another. Though the results were not as expected, valuable insights have been gained about the design of similar structures and where improvements can be made in future research, such as material selection and experimental setup.

The nominal difference between the modal frequencies from the experiments to those of the model and theory is interesting to note as well due to the vast magnitude. The first mode frequency found experimentally was around 15-20Hz for all tests, while the first mode frequency estimated analytically and numerically was around 63-67Hz, nearly 2.5 times greater. Because the property values used in the theoretical calculations and the model were the same and the resulting natural frequencies found were also close, the issue is likely in the material properties and dimensions used. Primarily, the carbon fiber beam dimensions were measured

and the thicknesses were found to be inconsistent around the cross-section and marginally different from the published value that was used in the model and calculations. Furthermore, the isotropic and elastic assumptions for the carbon fiber composite are certainly possible causes for error and tensile tests would be much better at determining appropriate values.

After modeling and testing, the modulus of elasticity used for silicone was determined to be incorrect and a more accurate value was found. Despite this, when the theoretical calculations were fixed with the new value, the resulting natural frequencies changed by less than 0.01%, from 66.6974 to 66.6967. This is because the natural frequency of the silicone alone was so low already that most of its effect on the structure's natural frequency at room temperature was due to the distributed mass that it adds.

It is also possible that assuming the rounded corners of the carbon fiber as square caused some errors. While theoretically, the values of the moment of inertia are nearly the same, the physical layup of the carbon fiber in this way may change the structural properties and the way that stresses are distributed. Another source of error is that the experimental specimens were the same length as the model but the clamped boundary conditions were different. The clamp effectively shortened the length of the cantilever; however, this should have actually raised the measured frequency rather than lowering it.

Furthermore, effects from how strong the adhesion was between the carbon fiber and multiphase material may have come into play as well, such as that connection changing upon the melting of the wax. It was noticed in manufacturing the multiphase material that the silicone pulls easily away from the mold while the silicone mixed with wax sticks stubbornly until heated and the wax at the surface melts.

A thermal camera was used to qualitatively show the temperature distribution. This turned out to be uneven in the specimens, meaning that modifications to the heating and testing process would also likely improve future results. Due to time and resource limitations, further study to match the models and theory to the experiments better was not possible.

Chapter 5
CONCLUSION

In this work, the dynamic performance of aerospace structures with embedded multiphase materials was reported. The feasibility of tunable stiffness and damping parameters using these methods were researched in a proof of concept. In order to combat the harmful effects of environmental and operational damage on aerospace structures, a novel method was proposed to redirect thermal energy. The thermal energy generated from aerodynamic heating would be used to create internal pressure by using phase change expansion. This proof of concept showed that structures could be programmed dynamically to mitigate vibratory loads. Experimental tests were presented that characterized the multiphase materials, demonstrated stiffness and damping tuning with heat, and provided a comparison between using single-phase and two-phase materials in this concept. Validation was provided by the use of analytical calculations and numerical models. It was shown that the increase in internal thermal pressure with a change of 30K increased the damping of the structure by 50% while counteracting the natural drop in stiffness that occurs with temperature increase. This demonstrates the potential for a way forward with multiphase material as a tool for tuning modal properties.

5.1 Future Revisions to Analysis

To ensure similarity between the model and experiment, in future testing all materials should be confirmed to have the expected properties and dimensions before using them in any modeling or calculations. Similarly, precision in models should not be ignored. For example, with time permitting, the models should have been run again with appropriate dimensions, masses, and materials after the experimental tests were conducted. In this case, the models

were completed first and then the experiments were conducted. While this was good practice in order to find estimated values and determine if the experiments are worth conducting, some changes were made to the design such as using milled PVC and bolts for the end caps rather than carbon fiber glued flush to the end. This primarily changed the tip mass which affects the vibration results to a significant degree. For the purpose of this study, the results are still valid when comparing the normalized modal frequencies from the experiment with those from the analysis.

Another change made after the models were completed was the cantilever setup itself. Due to the design of the clamp and other considerations, the length of the beam that was actually cantilevered was less than the total 60cm. The clamp on top and bottom would ideally be modeled properly in the numerical study, rather than the boundary condition used in the model where the flat end of the beam was fixed.

While not necessary for the purposes of this thesis, it would be more accurate to combine the thermal distribution and thermal expansion models into one that simulates the heating process in its entirety. This separation was done for simplicity purposes and to keep the results separate and easier to understand individually, but an additional model would potentially help show how the distribution of temperature within the multiphase material affects the stiffness.

5.2 Future Revisions to Experiments

In future studies, it would be best to conduct heating at slower rates and cover it with a cardboard box or similar for insulation against air convection. This would allow temperature distributions in all studies to be more consistent and homogeneous throughout each specimen. It would also be possible to use an alternative method of heating such as an oven for a similar effect.

Measurements of the specimen dimensions before, during, and after the tests would be useful to understand the true changes in the second moment of area in the cross-section as well as how much expansion is actually seen experimentally versus the model. These would

also indicate if there is any over-stressing of the carbon fiber composite. On a similar note, strain gauges would be useful to include on the specimens to see what kinds of stresses and strains are occurring with the expansion from increases in temperature and compare those with the model as well.

5.3 Future Work Beyond Concept

Future work on this research should begin with expanding upon the current data and determining further reasons for the differences between numerical and experimental analysis. Additional compositions of silicone and wax should be tested with higher weight percentages of wax. Alternative beam shell materials to carbon fiber composite could be used as well. Future work should be focused on continuing to demonstrate that a viable concept has been successfully developed before moving on to testing for specific uses and designs with more complicated structures. To that end, experimental and numerical testing could be done on modeled aircraft wings and full-body structures to see changes in stiffness and damping. Strategically placed multiphase materials could be incorporated. These models could then be tested in a physical or simulated wind tunnel to determine how heating affects aeroelasticity.

While there is a long way to go before this concept would reach a production aircraft, the first steps have now been taken.

BIBLIOGRAPHY

H, A., and Pai, P. F. N., *Linear and nonlinear structural mechanics*, John Wiley & Sons, 2008.

"Braided Carbon Fiber Rectangular Tubing," , 2023a. URL https://dragonplate.com/braided-carbon-fiber-rectangular-tubing-2-x-1-x-48.

"Mechanical Properties of Carbon Fibre Composite Materials," , 2023b. URL http://www.performance-composites.com/carbonfibre/mechanicalproperties_2.asp.

"Carbon Fiber Thermal Conductivity and the Coefficient of Thermal Expansion," , 2021. URL https://dragonplate.com/carbon-fiber-thermal-conductivity-and-the-coefficient-of-thermal-expansion.

"Product Overview: Mold Max™ 14NV and 29NV Mold Max™ 14NV and 29NV Low Viscosity Tin Cure Silicone Rubber Compounds Low Viscosity Tin Cure Silicone Rubber Compounds," , 2023. URL www.smooth-on.com.

"Overview of materials for Silicone Rubber," , 2023. URL https://www.matweb.com/search/datasheet.aspx?matguid=cbe7a469897a47eda563816c86a73520&n=1.

"Mechanical Properties of Wax," , 2023. URL https://material-properties.org/wax-properties-application-price/.

"Paraffin wax emulsion," , 2023. URL https://www.matweb.com/search/datasheet.aspx?matguid=07af9341394541779a950f0a5bd13b16&ckck=1.

"Thermal Conductivity of Carbon Fiber, and other Carbon Based Materials," ,

2023c. URL https://www.christinedemerchant.com/carbon_characteristics_heat_conductivity.html.

"Paraffin wax thermal properties," , 2023.

Habtour, E. M., Cole, D. P., Kube, C. M., Henry, T. C., Haynes, R. A., Gardea, F., Sano, T., and Tinga, T., "Structural state awareness through integration of global dynamic and local material behavior," *Journal of Intelligent Material Systems and Structures*, Vol. 30, 2019, pp. 1355–1365. https://doi.org/10.1177/1045389X19828489.

Habtour, E., Maio, D. D., Masmeijer, T., Gonzalez, L. C., and Tinga, T., "Highly Sensitive Nonlinear Identification to Track Early Fatigue Signs in Flexible Structures," *Journal of Nondestructive Evaluation, Diagnostics and Prognostics of Engineering Systems*, Vol. 5, 2022. https://doi.org/10.1115/1.4052420.

Zhao, Y. H., "Flutter suppression of a high aspect-ratio wing with multiple control surfaces," *Journal of Sound and Vibration*, Vol. 324, 2009, pp. 490–513. https://doi.org/https://doi.org/10.1016/j.jsv.2009.02.026, URL https://www.sciencedirect.com/science/article/pii/S0022460X09001783.

Butaud, P., Renault, D., Verdin, B., Ouisse, M., and Chevallier, G., "In-core heat distribution control for adaptive damping and stiffness tuning of composite structures," *Smart Materials and Structures*, Vol. 29, 2020.

Mann, A., Germann, T., Ruiter, M., and Groche, P., "The challenge of upscaling paraffin wax actuators," *Materials and Design*, Vol. 190, 2020. https://doi.org/10.1016/j.matdes.2020.108580.

Lipton, J. I., Angle, S., Banai, R. E., Peretz, E., and Lipson, H., "Electrically Actuated Hydraulic Solids," *Advanced Engineering Materials*, Vol. 18, 2016, pp. 1710–1715. https://doi.org/https://doi.org/10.1002/adem.201600271, URL https://onlinelibrary.wiley.com/doi/abs/10.1002/adem.201600271.

Gürgen, S., and Sofuoğlu, M. A., "Experimental investigation on vibration characteristics of shear thickening fluid filled CFRP tubes," *Composite Structures*, Vol. 226, 2019. https://doi.org/10.1016/j.compstruct.2019.111236.

Agnese, F., and Scarpa, F., "Macro-composites with star-shaped inclusions for vibration damping in wind turbine blades," *Composite Structures*, Vol. 108, 2014, pp. 978–986. https://doi.org/10.1016/j.compstruct.2013.10.030.

Arani, A. G., Shajari, A. R., Atabakhshian, V., Amir, S., and Loghman, A., "Nonlinear dynamical response of embedded fluid-conveyed micro-tube reinforced by BNNTs," *Composites Part B: Engineering*, Vol. 44, 2013, pp. 424–432. https://doi.org/10.1016/j.compositesb.2012.04.025.

Xia, Y., Chen, B., Weng, S., Ni, Y.-Q., and Xu, Y.-L., "Temperature Effect on Vibration Properties of Civil Structures: A Literature Review and Case Studies," , 2012.

Whitney, S., "Vibrations of Cantilever Beams," , 1999. URL http://emweb.unl.edu/Mechanics-Pages/Scott-Whitney/325hweb/Beams.htm.

"Paraffin Wax, 1 lb. Beads McMaster-Carr," , 2023.

Wiersinga, P., Sleavin, A., Boom, B., Masmeijer, T., Flint, S., and Habtour, E., "Hybrid Compliant Musculoskeletal System for Fast Actuation in Robots," *Micromachines*, Vol. 13, 2022. https://doi.org/10.3390/mi13101783.

"PVC Properties," , 2018.

"Safety Data Sheet SDS No. 823A," , 2021. URL www.smooth-on.com.

"Coefficient of Thermal Expansion for Various Materials at Different Temperatures," , 2004. URL www.balseal.com.

Safaeifar, H., and Karimi, A., "The Effect of Temperature on the Natural Frequency," 2015.

Esfarjani, S. M., Salehi, M., and Ghassemi, A., "Effect of the multiple damages and temperature changes on the natural frequency," *Journal of Theoretical and Applied Mechanics (Poland)*, Vol. 55, 2017, pp. 813–822. https://doi.org/10.15632/jtam-pl.55.3.813.

Meirovitch, L., *Fundamentals of vibrations*, McGraw-Hill, 2001.